3-26-2015

Energy Harvesting & Recapture from Human Subjects: Dual-Stage MEMS Cantilever Energy Harvester

Nicholas P. Sullivan

ENERGY HARVESTING & RECAPTURE FROM HUMAN SUBJECTS: DUAL-STAGE MEMS CANTILEVER ENERGY HARVESTER

THESIS

Nicholas P. Sullivan, Second Lieutenant, USAF

AFIT-ENG-MS-15-M-068

DEPARTMENT OF THE AIR FORCE
AIR UNIVERSITY

AIR FORCE INSTITUTE OF TECHNOLOGY

Wright-Patterson Air Force Base, Ohio

AFIT-ENG-MS-15-M-068

ENERGY HARVESTING & RECAPTURE FROM HUMAN SUBJECTS: DUAL-STAGE MEMS CANTILEVER ENERGY HARVESTER

THESIS

Presented to the Faculty

Department of Electrical and Computer Engineering

Graduate School of Engineering and Management

Air Force Institute of Technology

Air University

Air Education and Training Command

In Partial Fulfillment of the Requirements for the

Degree of Master of Science in Electrical Engineering

Nicholas P. Sullivan, BS

Second Lieutenant, USAF

March 2015

AFIT-ENG-MS-15-M-068

ENERGY HARVESTING & RECAPTURE FROM HUMAN SUBJECTS: DUAL-STAGE MEMS CANTILEVER ENERGY HARVESTER

Nicholas P. Sullivan, BS

Second Lieutenant, USAF

Committee Membership:

Brett J. Borghetti, PhD
Chair

Ronald A. Coutu Jr., PhD
Member

Derrick Langley, Maj, USAF, PhD
Member

AFIT-ENG-MS-15-M-068

Abstract

Recent thermal energy harvesting research has advanced alternative non-Seebeck devices and shifted attention towards applications with low temperature differentials near ambient. This research effort takes a simulation-based approach to improve the performance of a modified dual-stage MEMS cantilever energy harvester. The device employs a bimetal and a piezoelectric transducer to harvest energy from a 10 °C temperature differential. The proposed application for the device is as a wearable energy harvester, capable of generating power from the human body using skin temperature (average 33 °C) as the hot side and ambient air (23 °C) as the cold side. A bimetal thickness scaling study is conducted, in which the 1.5 μm bimetal thickness yields the maximum electrical power output of 36.82 nW per device. This translates to a power density of 5.68 mW/cm^2, which surpasses the performance of many Seebeck and non-Seebeck designs from the literature.

Acknowledgments

I would like to express my sincere appreciation to my faculty advisor and committee members for their guidance and support throughout the course of this thesis effort. I would also like to thank the 15M AFIT MEMS Group members and the Cyber ANiMaL Group members for the insight and feedback they provided. Finally, I thank the LORENet support staff for their dedication in meeting the needs of the researchers.

Nicholas P. Sullivan

Table of Contents

Page

Abstract iv
Acknowledgments v
Table of Contents vi
List of Figures viii
List of Tables x
I. Introduction 1
General Issue 1
Problem Statement 4
Research Objectives 5
Investigative Questions 6
Methodology 6
Assumptions/Limitations 7
Implications 8
Preview 8
II. Literature Review 10
Chapter Overview 10
Relevant Research 10
Kinetic Energy Harvesting 14
Seebeck Thermal Energy Harvesting 21
Non-Seebeck Energy Harvesting 27
Derivation 34
Summary 40
III. Methodology 43

Chapter Overview 43
Experiment Design 43
Summary 55
IV. Analysis and Results 56
Chapter Overview 56
Larger Bimetal Thicknesses 57
Smaller Bimetal Thicknesses 65
Aggregate Results 71
Summary 75
V. Conclusions and Recommendations 76
Chapter Overview 76
Design Configuration 76
Control Variables 77
Significance of Research 80
Recommendations for Future Research 80
Summary 82
Appendix 83
Bibliography 85

List of Figures

Figure 1. Methods that heat escapes from human skin into ambient air 5

Figure 2. System block diagram view of a passive autonomous sensor [6] 11

Figure 3. System block diagram view of a self-powered autonomous sensor [6] 12

Figure 4. Vibrational energy harvesting system diagram [1] 15

Figure 5. (a) In-plane overlap-varying capacitive harvester, (b) In-plane gap-closing capacitive harvester, (c) Out-of-plane gap-closing capacitive harvester [1] 18

Figure 6. Through-plane thermoelectric array (top), In-plane thermoelectric array (bottom) [1] 23

Figure 7. Bimetal and electret based converter for thermal energy harvesting [22] 29

Figure 8. Improved design of bimetal and electret based converter for thermal energy harvesting [25] 30

Figure 9. Stability of Ti-Au bimetal strips (L = 200 μm) [26] 32

Figure 10. 2D layout of dual-stage MEMS cantilever energy harvester design 45

Figure 11. Boundary definitions of the dual-stage MEMS cantilever energy harvester 46

Figure 12. Expanding active bimetal layer (deformation scale 500; PZT layer not shown) 57

Figure 13. 5 μm thick bimetal cantilever tip displacement 58

Figure 14. 5 μm thick bimetal cantilever voltage signal 59

Figure 15. Stressed piezoelectric material (deformation scale 500; bimetal layer not shown) 61

Figure 16. 5 μm thick bimetal cantilever current density 62

Figure 17. 5 μm thick bimetal cantilever instantaneous power 63

Figure 18. 1.5 μm thick bimetal cantilever tip displacement....66
Figure 19. 1.5 μm thick bimetal cantilever voltage signal....67
Figure 20. Stressed piezoelectric material (deformation scale 100; bimetal layer not shown)....68
Figure 21. 1.5 μm thick bimetal cantilever current density....69
Figure 22. 1.5 μm thick bimetal cantilever instantaneous power....70
Figure 23. Peak voltage versus bimetal thickness across all simulations....72
Figure 24. Cantilever beam frequency versus bimetal thickness across all simulations..73
Figure 25. Average power versus bimetal thickness across all simulations....74
Figure 26. 1 μm bimetal thickness simulation experiencing an inflection point (bimetal not shown)....78

List of Tables

Table 1. Parameter Evolution from Dimension Down-Scaling [4].....33

Table 2. Summarized list of performance metrics for the surveyed energy harvesters ...42

Table 3. Variable Summary.....53

Table 4. Test Matrix.....54

ENERGY HARVESTING & RECAPTURE FROM HUMAN SUBJECTS: DUAL-STAGE MEMS CANTILEVER ENERGY HARVESTER

I. Introduction

General Issue

Energy harvesting is a process of capturing energy from a system's surrounding environment and converting it into usable electrical power. This field of research continues to draw the attention of the academic community as its applications are extensive and its topics are multi-disciplinary. The most common sources of energy that are exploited for power generation in energy harvesting systems include temperature differentials, kinetic energy, radio frequency energy, solar energy, and biochemically produced energy. The current study focuses on only one unique application of thermal energy harvesting from small temperature differentials. The details of this unique application will be described explicitly in the *Problem Statement* subsection of this chapter.

There are three critical phases in an energy harvesting system: energy collection, energy conversion, and energy storage. The energy collection component of the system transforms the energy present in the surrounding environment into some form of electrical power. The output of the energy collection component feeds into the input of an energy conversion component. The energy conversion component of the system converts one kind of electrical power into a different—but more useful—kind of electrical power. Often, the energy conversion component provides an appropriate amplitude DC voltage at its output that is independent of the electrical power waveform

seen at its input. The output of the energy conversion component feeds into the input of an energy storage component. The energy storage component of the system accumulates the power collected by the energy harvesting system for use at a later time. It may be common for energy harvesting systems to generate power intermittently over a period of time; thus, the energy storage component can compensate for this aspect of device behavior by delivering continuous power. These three components form an energy harvesting system and enable a self-sufficient device. The current study focuses only on thermal energy harvesting, which falls under the category of an energy collection component. This information about the three critical phases provides a context for the research conducted in this study and significance for the inputs and outputs of the device.

Thermal energy harvesting has existed for many years as a reliable power generation method [1]. Most past research investigates applications of thermal energy harvesting in systems that have large temperature differentials, such as industrial processes, vehicle exhaust, and space travel. This research paradigm shifted its attention to applications concerning room temperature ambient sources with much lower temperature differentials in the past decade. Additionally, a high percentage of past thermal energy harvesting research examines Seebeck devices. The Seebeck Effect describes a material property that produces a voltage potential directly from an applied temperature gradient. The generation of a voltage potential is possible in certain materials because charge carriers in a conducting material tend to flow in the direction of the temperature gradient. This property is quantified by the Seebeck coefficient, which has units of volts per Kelvin [V/K]. Semiconductor materials have displayed the most

desirable qualities by exhibiting high Seebeck coefficients and have consequently been the primary focus of research for thermal energy harvesting.

Electrical conductivity and thermal conductivity are two crucial material properties that govern the device performance for thermoelectric systems [1]. Electrical conductivity is defined as the degree to which a material can conduct an electrical current. Thermal conductivity is defined as the rate at which heat passes through a material. The electrical conductivity needs to be maximized and thermal conductivity needs to be minimized for the best performance in Seebeck devices. Thermal conductivity is divided into two components: the phonon transport component and the electrical component of thermal conductivity. Due to the Wiedemann-Franz Law, the electrical component of thermal conductivity is proportional to overall electrical conductivity, which poses a problem for finding materials with a high thermoelectric figure of merit (a characterization metric based on the Seebeck coefficient). Bismuth Telluride (Bi_2Te_3) is the most commonly used thermoelectric semiconductor material and adequately accommodates conventional microfabrication methods.

Non-Seebeck thermal energy harvesting is a different branch of research that does not involve the use of semiconductor materials for direct voltage generation. Non-Seebeck devices employ a myriad of other innovative methods to generate a voltage from a thermal gradient. The current study examines one particular non-Seebeck dual-stage thermal microelectromechanical system (MEMS) energy harvesting design demonstrated by Puscasu *et al.* and presents a cantilever-based variation on the design [2, 3, 4, 5]. This design, by Puscasu *et al.*, employs a bimetal that works in conjunction with a piezoelectric membrane. The bimetal operates by first converting thermal energy

to mechanical energy. The piezoelectric membrane captures the mechanical energy of the bimetal and then converts it to electrical energy. By this method, the dual-stage MEMS energy harvesting design implements a two-stage energy conversion process to generate power. A detailed description of dual-stage thermal energy harvesting device operation is included in the *Literature Review* chapter of this document.

Problem Statement

The problem that this thesis research addresses is whether Puscasu's design for thermal energy harvesting can be improved and successfully applied to human subjects. The human body can be regarded as a source of heat and therefore a power source for thermal energy harvesting devices. Human-powered energy harvesting devices grant the convenience of a mobile platform that can supply electrical power. Being warm-blooded mammals, human body heat is generated from within by normal cell function and escapes through the epidermis by way of conduction, convection, radiation, and evaporation. Figure 1 shows the methods by which thermal energy escapes from human skin into ambient air.

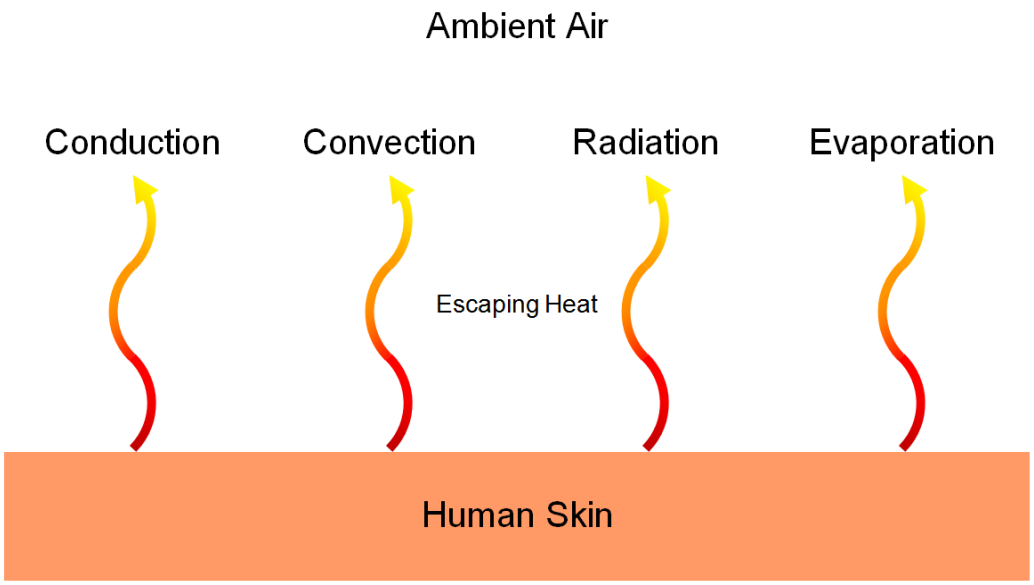

Figure 1. Methods that heat escapes from human skin into ambient air

A properly designed thermal energy harvesting device captures and repurposes this outward heat flow from a portion of the human body and uses it to produce electrical power. The current study will investigate modified dual-stage thermal energy harvester operation designed for human use through modeling and simulation. The end goal is to simulate a wearable thermal harvesting device able to produce sufficient electrical power to operate a biomedical sensor or charge an electronic device. Shared interest exists for creating a thermal energy harvesting device with these capabilities.

Research Objectives

One objective of this research is to surpass the capabilities of similarly implemented Seebeck devices under the same conditions. The other objective of this research is to create an improved design that surpasses the performance of the non-Seebeck designs recorded in the *Literature Review*. The measures of success for this

research seek to show how Puscasu's scaling assumptions hold for the modified thermal energy harvesting design; the measures of success for this research also seek to outperform Seebeck power generation under the conditions of the human environment. The conditions of the human environment for this research are defined by a thermal gradient that uses 33 °C as the hot side temperature and 23 °C as the cold side temperature. The standard for power density among Seebeck devices varies drastically, but for this research, the threshold for Seebeck power densities is to be considered ~1 mW/cm^2. The main foci for this research include cantilever displacement, oscillation frequency, peak voltage, power density, and overall device performance. Dimensional downscaling/device miniaturization is the primary means that this research uses to improve device performance. Appropriate thermal management, a useful temperature operating range, and reliability are crucial aspects of favorable device performance. Device size, weight, and flexibility are important factors governing the overall mobility of the design.

Investigative Questions

Can a dual-stage thermal energy harvesting design be improved to surpass the performance of current Seebeck and non-Seebeck thermal energy harvesting technology? Can a dual-stage thermal energy harvesting design be adapted to operate in temperature gradients that humans normally exhibit?

Methodology

This research effort uses a simulation-based approach to achieve design improvement; the software employed is COMSOL® Multiphysics, an industry-recognized

and versatile simulation platform. After identifying the key parameters to vary that are consistent with the literature, a series of simulations are conducted to observe the effects of the varying parameters and draw conclusions from the results.

Assumptions/Limitations

The assumptions and limitations in this research effort mainly involve the computer simulation of the improved design. As in any simulation effort, the applicability to real-world systems or characteristics depends on the validity and accuracy of the employed models in the software. The software used in this research effort is the COMSOL® design and simulation platform, which is a commonly used and experimentally validated tool for MEMS devices and many other applications. Therefore, the COMSOL® simulation tool is assumed to employ accurate numerical models from a theoretical basis to match the real-world operation of simulated devices.

One of the main design improvement techniques that are employed in this research is dimensional downscaling or device miniaturization. COMSOL®, being a simulation tool often used for MEMS applications, is expected to maintain accuracy in its calculations over a wide range of scalability. For real-world devices, non-idealities become prominent as device dimensions push the limits of scalability. Although a well-reasoned mathematical derivation from the literature has predicted improved device performance for a fixed area as the device dimensions are scaled down, there will be a point of diminishing returns in the real world where non-idealities will inhibit the perpetual increase in device performance [2]. The heat flux across the device is also expected to increase as the device dimensions are decreased; for the purposes of this

experiment, it will be assumed that the original applied temperature gradient will be maintained across the device regardless of scaling.

Implications

The motivation for human-based energy harvesting research is to provide mobile stand-alone systems that will function as a source of power where a connection to the power grid is infeasible. One main goal is to reduce dependence on batteries. The downscaling of battery-dependent system components causes the size and weight of the system to be chiefly determined by the battery itself [1]. Opportunity exists for military application as this technology may replace the need for fielded military to carry unwieldy batteries to power their equipment. This body of research also seeks to contribute towards the movement for "greener" energy and reduced reliance on conventional power production. The expenditure of heat energy already takes place in both natural human function and in the surrounding environment; systems that exploit this un-used thermal energy provide a unique mobile charging platform for self-sufficient physiological monitoring or electronics charging through the means of a wearable energy harvesting device. This field of research has caught the attention of many who seek to advance environmentally-friendly energy production technology and battery-less systems.

Preview

The succeeding portions of this document adhere to the following structure order: Chapter 2 will present the literature and theory review from past relevant contributions; Chapter 3 will present the methodology of the simulation; Chapter 4 will present the data

and analyze the findings; Chapter 5 will present the results of this thesis research, draw conclusions based upon the data, and suggest future work.

II. Literature Review

Chapter Overview

The rationale for a new investigation on dual-stage thermal MEMS energy harvesters stems from the past work conducted by researchers within the thermal energy harvesting field. The subfield of non-Seebeck thermal energy harvesting methods is relatively new in concept and lacks a comprehensive collection of previously conducted research. This chapter starts with a broad description of energy harvesting systems and gradually narrows the scope of the literature discussed to non-Seebeck thermal energy harvesting devices. There is one primary team of researchers that is studying dual-stage thermal MEMS energy converters, and much of the mentioned relevant work toward the end of this chapter is comprised of its findings. This chapter exhibits portions of previous relevant research and explains the resultant implications that drive the direction of this thesis effort. Finally, the chapter closes with a summary of the implications extracted from the literature.

Relevant Research

The relevant research section begins by discussing a broad range of energy collection and ends by focusing on the relevant research that is most comparable to the current study. A topographical analysis of energy harvesting systems gains relevance if a discussion of terminology is first articulated to justify the significance of topics discussed later in this document.

A discussion of passive and self-powered autonomous sensor systems follows. An autonomous sensor is defined as a device that autonomously performs measurement

functions within its environment [6]. Passive autonomous sensors imply passive circuit elements and passive operation; self-powered autonomous sensors imply the use of an energy harvesting module. Autonomous sensors, though not the main focus of this document, serve as a context medium for energy harvesting because they are common miniaturized systems that record data. Figure 2 shows a block diagram of a passive sensor system.

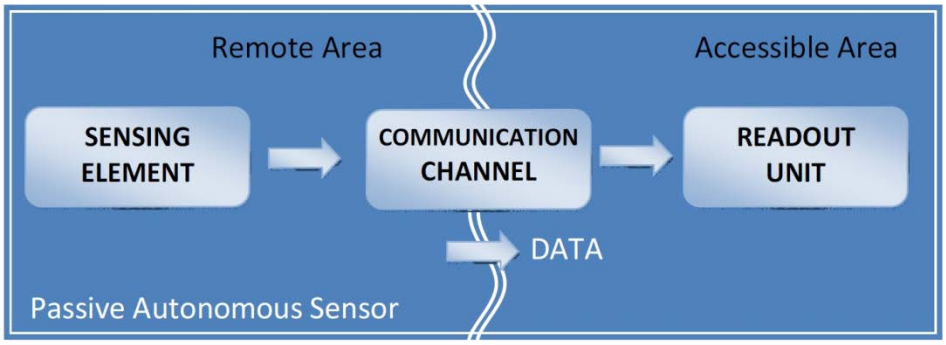

Figure 2. System block diagram view of a passive autonomous sensor [6]

The passive sensor system consists of a sensing element and a readout unit that are brought into proximity in order to form a communication channel. The communication channel bridges the barrier between the remote and accessible regions and the consequent data flow is mono-directional. The communication channel is formed only when the readout unit interrogates the sensing element because the sensing element does not provide power for itself nor does it have any type of power supply.

Self-powered autonomous systems observe a much different mode of operation than passive autonomous sensors in the remote area. Figure 3 shows a block diagram of a self-powered sensor system.

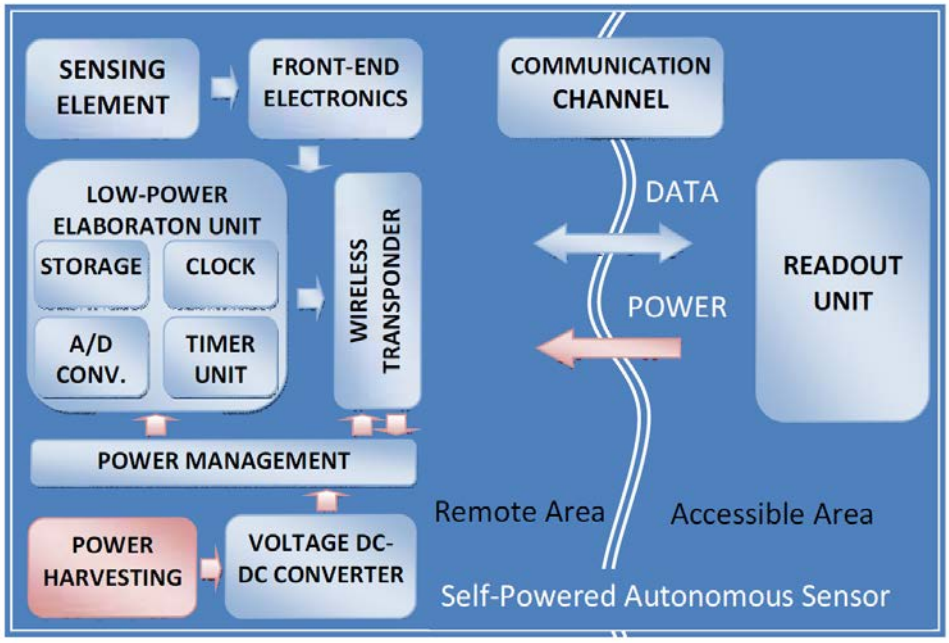

Figure 3. System block diagram view of a self-powered autonomous sensor [6]

The self-powered sensor system is an upgrade in complexity compared with the passive sensor system as indicated by the increased number of functions in the diagram. Similarities of the two autonomous sensors include the distinction between a remote and an accessible region of the system which is bridged by the communication channel to interface the readout unit. Data flow capabilities are bi-directional due to the wireless transponder. Power may also be supplied to self-powered sensor device by the readout unit, but only for the purposes of data transfer. The many blocks composing the self-powered sensor device in the remote region of the diagram form an independently functioning entity. In the absence of the readout unit, the device in the remote area is able to take measurements through the sensing element and store the data, all while providing its own power. The power is provided by the three energy harvesting components, which are the power harvesting block, the voltage DC-DC converter block,

and the power management block. These three blocks correspond to more generalized terms that describe the three phases of an energy harvesting system: energy collection, energy conversion, and energy storage, respectively. Energy collection components transform the energy present in the surrounding environment into electrical power. There are different sources of power that energy collectors can draw from including: thermal, vibrational, radiofrequency, solar, and chemical energy. These sources can either be drawn directly from the human body or harvested from the surrounding ambient environment through the means of a wearable device. The input of an energy conversion component is equivalent to the output of the electrical power from the energy collection component. Energy conversion components provide a usable DC output independent of the form of the electrical power seen at its input. The input of an energy storage component is equivalent to the output of the DC power from the energy conversion component. Energy storage components hold the power generated by the energy harvesting system for use at a later time. It may be common for energy harvesting systems to only intermittently generate power over a period of time; thus the energy storage component can compensate for this aspect of device behavior by delivering continuous power. These three components form an energy harvesting system and enable a self-powered autonomous sensor to be a self-sufficient entity. Discussions of common autonomous sensors types and the three phases of energy harvesting have been provided to lay a foundation for a more focused discussion of piezoelectric and thermal energy harvesting systems, which function as energy collection components.

The energy collection aspect of energy harvesting has seen the most emphasis in research efforts from the birth of this field of study. Many techniques have been

developed for exploiting different forms of energy in either ambient or controlled environments. It should be noted that device miniaturization is an important recurring theme for this particular application of energy harvesting. Although component miniaturization is relevant for all three phases of energy harvesting, unique principles that apply primarily to energy collection devices govern the scaling laws for centimeter-sized devices down to micron-sized devices. The significance of natural forces changes at the small-scale when compared to the macro-scale. Natural forces refer to surface tension, electrostatic, electromagnetic, and gravitational forces. When devices are scaled down and surface area to volume ratios increase, surface tension forces dominate inertial forces [7]. These are important considerations for miniaturized energy collection devices that make use of these forces to generate electrical power.

Kinetic Energy Harvesting

Vibrational or kinetic energy harvesting contains many subcategories composed of different harvesting methods. It is less suited to harvesting applications relating to humans due to its high resonant frequencies, but vibrational harvesting systems can be optimized for lower frequencies at the expense of other trade-offs. Figure 4 shows a generic vibrational system that communicates the essential elements of vibrational energy harvesting operation.

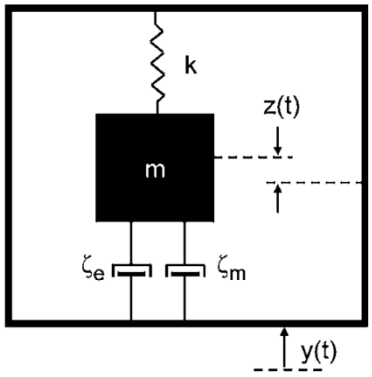

Figure 4. Vibrational energy harvesting system diagram [1]

Where *k* is the spring constant, *m* is the weight of the proof mass, ζ_e is the electrical damping coefficient, ζ_m is the mechanical damping coefficient, *z(t)* accounts for the movement of the proof mass, and *y(t)* accounts for the movement of the entire structure. Vibrational harvesters usually need to have a narrow bandwidth in order to generate appreciable power; therefore, vibrational harvesters must be designed to operate at their resonant frequency (fundamental frequency).

Electromagnetic vibrational harvesting is a common form of energy collection, but most electromagnetic systems have resonant frequencies much higher than would be suitable for human applications. Elliott and Zilletti present an analytical approach to harvesting energy from electromagnetic transducers purposed for shunt damping applications [8]. The goal of the analysis is to determine the relationship between the efficiency of an electromagnetic transducer and the coupling coefficient. It is demonstrated that the coupling coefficients scale approximately with the size of the electromagnetic transducer. By contrast, piezoelectric coupling coefficients are independent of the size of the piezoelectric transducer. Elliott's analysis shows that, based on the coupling coefficient, devices under 10 kg in weight should employ

piezoelectric transducers. Devices over 10 kg in weight should employ electromagnetic transducers. Therefore, the acute drawback in human applications is that miniaturized electromagnetic devices suffer great efficiency losses in comparison to equivalent piezoelectric systems. Efficiency losses in addition to increases in the resonant frequency as the size of the device is scaled down make electromagnetic vibrational energy harvesting a poor candidate for human applications.

Very low frequency energy harvesting operation is possible in a piezoelectric ring system. Xie *et al.* designs and simulates a macro-scale ring piezoelectric harvester with a diameter of about one meter [9]. Xie's research develops the harvester along with a mathematical model to predict the output of the device. The device is able to produce 12.7 W at a frequency of 1 Hz and is able to produce 381.7 W at a frequency of 30 Hz. Though this system is very large compared to the other devices surveyed in this document, it could be miniaturized without experiencing heavy efficiency losses because it is piezoelectric-based. Operation frequencies would increase with decreasing size, but it remains to be seen whether a small-scale piezoelectric ring harvester would be an effective device.

Capacitive or electrostatic harvesting is the most favorable vibrational energy harvesting method for human applications due to its ability to be fabricated with MEMS technology; but there are still inherent disadvantages to capacitive systems such as the need for a prior DC bias. Lin *et al.* creates and characterizes a dual cavity MEMS capacitor vibrational system through simulation and fabrication [10]. Lin executes finite element modeling (FEM) to characterize the motion and output of the MEMS capacitor. Simulations determine an optimally resonant frequency of 487 Hz; experimental data

determines the device resonant frequency to be 500 Hz. The maximum power generation of the fabricated capacitor array is able to reach 2.5 μW under conditions of high voltage bias (15 V) and extreme excitation accelerations (>5 Gs). Lin's design needs to operate at a lower frequency, with lower voltage bias, and much lower excitation accelerations if any application to human-based energy harvesting is to be realized. Lin also identifies squeeze film air damping as a future research effort that needs extensive characterization and numerical analysis. Squeeze film air damping is a surface tension effect that becomes substantial as the size of micro-machined structures is decreased [11]. The movement of mechanical parts encounters a counter-reactive force by compressing the surrounding air between parallel surfaces and thus affecting the frequency response of the system. These compression damping forces overshadow drag damping forces if the created air film is less than a third of the transverse dimension of the surface.

Capacitive energy harvesting, similar to thermal energy harvesting, is realizable in more than one orientation. The three orientations for capacitive harvesting have unique working qualities. Figure 5 shows the different orientations for capacitive energy harvesting that have been investigated previously.

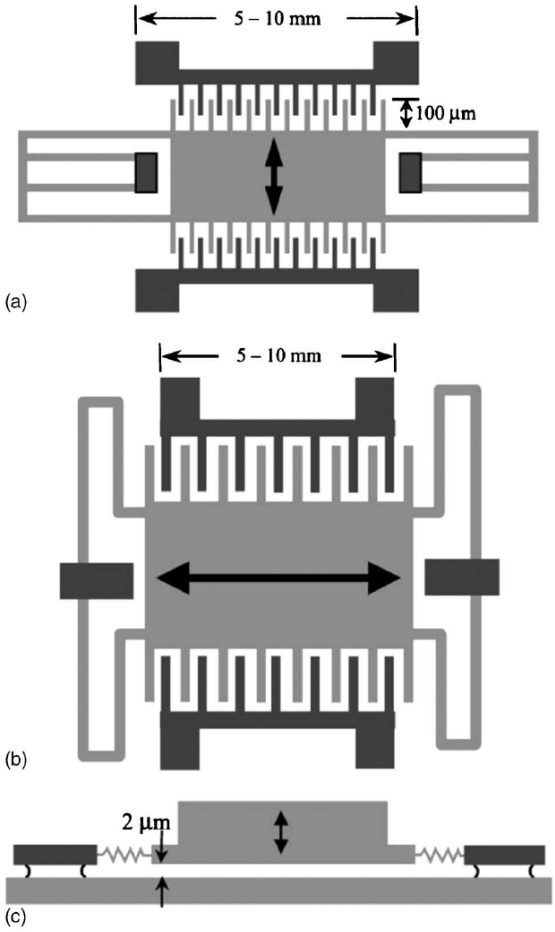

Figure 5. (a) In-plane overlap-varying capacitive harvester, (b) In-plane gap-closing capacitive harvester, (c) Out-of-plane gap-closing capacitive harvester [1]

The two-way arrows in each subpart of Figure 5 indicate the shuttle's direction of motion. With a prior applied voltage bias, the movement of the shuttle changes the capacitance and generates an output signal. One devised method of applying a permanent voltage bias is implementing an electret material. Electret materials eliminate the need for an external voltage source by maintaining a built-in electric field. Arakawa *et al.* proposed an in-plane overlap-varying capacitive harvester that has a fluorocarbon-based electret material with a high dielectric strength spun onto the electrodes [12]. The

fabrication of the capacitive device and the deposition of the electret material use common fabrication techniques. The device size is 20 mm × 20 mm × 2 mm and has a resonant frequency of 10 Hz. It produces 7.5 $\mu W/cm^3$ at an acceleration of 3.9 m/s^2. The low resonant frequency and low excitation acceleration of Arakawa's device make it a viable candidate for application to humans. If this work could be reproduced in an in-plane gap-closing orientation, then even lower excitation accelerations would produce the same output power because similar capacitances are attainable with reduced movement.

As previously mentioned, resonant frequency increases as the size of the device decreases. Non-resonant vibrational energy harvesting systems are one way that the negative effects of vibration energy harvesting device miniaturization can be avoided. Shenck and Paradiso created an impact-coupled system by implanting pre-stressed metal strips with PZT in the heels of shoes so that the act of walking would generate power [13]. At a frequency of 0.9 Hz, an average power of 8.4 mW is produced. Within the field of vibrational energy harvesting, impact-coupled, non-resonant devices may be the best suited to human application. Typical human movements do not exceed more than a few Hertz, yet the overall kinetic forces are much higher than other kinds of ambient vibrations. Caliò *et al*. have studied motion-based piezoelectric energy harvesting techniques and report the available power for a few human activities [14]. The available power from walking is ~1 W; the available power from breathing is ~100 mW; the available power from the upper limbs is ~10 mW; the available power from typing is ~1 mW.

A simulation effort in COMSOL® by Varadrajan and Bhanusri has attempted to maximize the power output in a macro-scale unimorph piezoelectric cantilever beam energy harvesting system [15]. The authors vary the design parameters of the unimorph piezoelectric cantilever beam and test three different piezoelectric materials: $PbZrTiO_3$ (PZT), PVDF, and PMN-PT. The beam length of Varadrajan and Bhanusri's design is 6 cm; the beam width is 3 cm; the beam thickness is 0.1 cm. A large proof mass is mounted on the tip of the cantilever beam to lower the fundamental resonant frequency, to decrease damping, and to increase the output power. With the addition of the proof mass, the fundamental resonant frequency is reduced to 153.22 Hz, which satisfies the author's target to fall within the frequency range of common environmental vibrations between 60 Hz and 200 Hz according to their sources. Varadrajan and Bhanusri report that varying the cantilever beam thickness has the greatest impact on the frequency of the device in comparison to varying strictly the length or the width. They conclude that frequency is directly proportional to the thickness of the beam from the results of their simulations.

Boisseau *et al.* report their findings on an electret-based cantilever energy harvester [16]. The authors conducted an optimization study on an electret-based cantilever energy harvester and determined from both theory and simulation that the maximum power they could achieve is 160 μW with a vibration amplitude of 10 μm at 50 Hz. The dimensions of the cantilever are 30 mm × 13 mm × 0.3 mm for the length, width, and thickness, respectively. The experimental results for the power output are much lower than anticipated due to parasitic capacitances. The load is reduced from 2.2 GΩ down to 300 MΩ to reduce the effect of parasitic capacitances. Boisseau obtains

an output power of 50 μW with a vibration amplitude of 10 μm at 50 Hz at low ambient vibrations accelerations of 0.1 g. It is concluded that parasitic capacitances have a large impact on the behavior of the electret-based cantilever energy harvester and greatly depend on the load chosen.

A discussion of thermal energy harvesting devices follows. Both Seebeck and non-Seebeck devices are discussed to convey the differences between these two technologies. Human-powered devices are also included in this review to articulate the challenges of operating thermal harvesting devices under constrained conditions.

Seebeck Thermal Energy Harvesting

It has been demonstrated that thermoelectric systems can be created using common fabrication techniques that are compatible with other wafer-based technologies. Bismuth Telluride (Bi_2Te_3), a common Seebeck thermoelectric material, is able to be processed using conventional fabrication methods. Böttner *et al.* uses physical vapor deposition and photolithography to pattern the p-type and n-type thermoelements on two separate substrates [17, 18]. Through a sequence of sputtering and patterning steps, Böttner builds $20 \times 40 \times 80$ μm^3 thermoelements and connects them in series with metal interconnects. The separate substrates are merged using flip-chip bonding, which is a popular procedure for thermoelectric devices due to the nature of alternating p-type and n-type thermoelement matrices. The resulting device produces a power density of 60 $\mu W/cm^2$ with a temperature differential of 5 K. The power density of this device is limited by the poor length to cross-sectional area ratio of the thermoelements. Thermoelement dimensions are factors that significantly impact the performance of

thermoelectric devices, which consequently produces a low power density in Böttner's research effort.

Device orientation is a novel geometrical effort that attempts to maximize the length to cross-sectional area ratio. As mentioned in the description of Böttner's work, the thermoelement geometrical dimensions influence the power density output. Ideally, the thermoelement dimensions can contribute positively to the power density if the length is much greater than the cross-sectional area dimensions. Conventional fabrication techniques are limited to depositing films not greater than a few hundred microns. Therefore, one proposed bypass to this issue is changing the device orientation from a through-plane orientation device to an in-plane orientation thermoelectric device. Many researchers have explored the usage of the in-plane orientation as a means of obtaining large aspect ratios in thermoelement geometry. Figure 6 shows two different orientations of thermoelectric arrays.

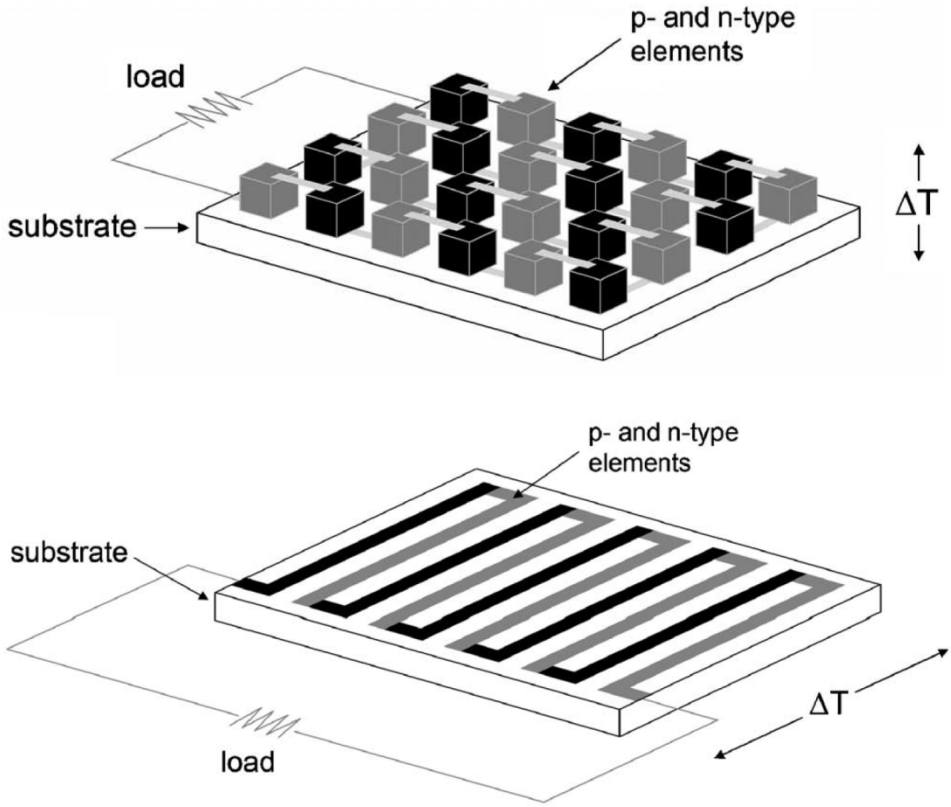

Figure 6. Through-plane thermoelectric array (top), In-plane thermoelectric array (bottom) [1]

In Figure 6, the indication of the direction of temperature flow is denoted by ΔT, which represents the temperature differential. Böttner's research, described above, is a through-plane orientation device. An example of notable mention is a design from Glosch *et al.* which describes an in-plane orientation thermoelectric device [19]. Glosch attempts to present a simplistic thermal harvesting design that contains high aspect ratio thermoelements. Glosch comprises the thermocouples of doped regions of c-silicon and aluminum connecting strips to act as the p-type and n-type elements. The use of aluminum connecting strips circumvents the need to create complimentarily n-type doped thermoelements, which simplifies the fabrication process. Both the aluminum strips and

the substrate itself are intentionally thin by design to prevent thermal shorting. At a temperature difference of 4 K, the device produces 0.2 μW with thermoelement dimensions of 500 × 7 × 1.2 μm^3. Requirements differ for through-plane orientation versus in-plane orientation devices. The former must have a high thermal conductivity substrate; the latter must have a low thermal conductivity substrate or a removable substrate. Glosch's design suffers from parasitic heat flow which greatly reduces the efficiency and overall performance of the thermoelectric device. Fabrication simplicity and a large thermoelement aspect ratio are the strongest points of Glosch's design. Future revisions to this work need to address parasitic heat flow issues so that the large thermoelement aspect ratio can be fully capitalized upon.

Thermoelectric materials research has yielded significant breakthroughs in figure of merit values for thermoelectric systems. Thermoelectric materials research focuses on restricting the transport of phonons in the device. Device performance improves when the thermal conductivity is minimized; therefore, research targets phonon management, which is a component of thermal conductivity. One way to restrict phonon transport is through low-dimensional materials, such as quantum wells, quantum wires, quantum dots, and superlattices [1]. One notable example of quantum confinement arises from Venkatasubramanian *et al.* by incorporating a superlattice structure into a room temperature thermoelectric device [20]. The p-type superlattice comprised of Bi_2Te_3/Sb_2Te_3 achieves a *ZT* value of 2.4 and the n-type superlattice comprised of $Bi_2Te_3/Bi_2Te_{2.83}Se_{0.17}$ achieves a *ZT* value of 1.2. These reported figures of merit are high when compared with other non-low-dimensional thermoelectric devices. The fabricated device boasts a power density of 6.1 mW/cm^2 at a temperature differential of

2.7 K. The superlattice functions as a low-dimensional material and scatters photons within the crystal structure to improve the figure of merit. Venkatasubramanian's device is only able to produce an output voltage of 42 mV, which is roughly an order of magnitude smaller than the majority of low-temperature thermoelectric devices.

One temperature-sensing self-powered autonomous sensor system that employs a thermoelectric module to harvest energy has been proposed and tested by Dalola *et al.* [21]. The system is designed to transmit the data via electromagnetic coupling when the readout unit comes within a distance of a few centimeters. When the readout unit is not in proximity to the self-powered autonomous sensor, the thermoelectric generator (TEG) provides power for the sensor to perform a temperature measurement and store the data in non-volatile memory. The system features a Seebeck TEG module that provides power for the autonomous sensor from a heat source. The induced voltage on the TEG feeds into the DC-DC boost converter, which provides a 2.1 V to the microcontroller and the RFID transponder. With the load connected, the temperature differential on the TEG must reach about 8.5 °C to produce a large enough input voltage (approximately 0.9 V) for the DC-DC boost converter to provide a stable output voltage of 2.1 V. The microcontroller and temperature sensor consume 0.9 mW of power from the TEG. Thus, Dalola's experimental results show a functioning self-powered autonomous temperature sensing system using a small temperature differential.

Hudak and Amatucci identify Seebeck thermoelectric devices to be the most conventional thermal harvesting method [1]. The most successful Seebeck materials are semiconductors; therefore, continuing investigation into microfabrication technologies and thermoelectric material science dominates conventional thermoelectric research. An

analysis of the governing power equations for Seebeck thermoelectric devices has sparked acute observance to device aspect ratios and maximum achievable power density. But despite the advances made in Seebeck Effect thermoelectric devices, there are inherent problems and disadvantages associated with procuring effective Seebeck materials, mainly related to the Wiedemann-Franz Law. Bismuth Telluride is an expensive material [22]. At room temperature, no bulk material has outperformed Bi_2Te_3 alloys; researchers are forced to evoke quantum material properties to surpass the figure of merit $ZT \sim 1$. Consequently, research concerning non-Seebeck thermal energy harvesting is being conducted. Non-Seebeck devices can circumvent the intrinsic problem of Seebeck devices, which is overcoming the strong link between semiconductor electrical properties and semiconductor thermal properties (Wiedemann-Franz Law).

Alternatively, other research efforts for direct thermoelectric applications to the human body are currently being investigated. Leonov experiments with the integration of Seebeck thermoelectric devices into human clothing for ambient temperature thermal energy harvesting applications [23]. Leonov's device is implanted into shirts to exploit the temperature differential between the human's skin temperature (typical 33 °C) and the ambient surrounding air (typical 23 °C). The implanted thermoelectric device has dimensions of a 5 mm thickness and a 3 cm diameter. Depending on the activity of the human subject (stationary or moving) and the ambient air temperature, the device generates an output power between 1 mW and 4 mW. Power generation is accomplished with a low heat flow rate, which does not cause discomfort to the human subject due to excessive parasitic heat flow. Leonov admittedly states that a more ergonomic design would improve the performance of his system. His system presents a competitive

alternative to battery use, but the cost of Seebeck thermoelectric systems is still an order of magnitude higher than the equivalent capability in the form of batteries; future research must close this gap in price and further miniaturize thermoelectric systems while still increasing power density.

Non-Seebeck Energy Harvesting

Regarding non-Seebeck research, the most relevant research to the current study is being conducted by a team of engineers from France. The authors mentioned in this literature review who are associated with this team of engineers include Puscasu, Monfray, Boisseau, and Arnaud.

Puscasu *et al.* initially propose an alternative MEMS-based heat energy harvesting device [2]. Puscasu's system employs a two-stage energy conversion: first from thermal energy to mechanical energy, then from mechanical energy to electrical energy. This two-stage conversion is realized using a preformed bimetal construct, which snaps between two stable states depending on its temperature. The bimetal snaps into an upward and downward position, periodically, to make mechanical contact with piezoelectric material that generates a voltage signal. The system still operates under the convention of having a hot side and a cold side (like all thermoelectric designs), but the mechanical movement of the bimetal beam transfers the heat. Scaling laws factor into the maximum power output of these devices because the researchers show that when the bimetal is reduced in dimension by a factor of k, the oscillation frequency is increased by a factor of k^2. Therefore, the proposed system benefits from miniaturization by a net factor of k.

In addition to bimetal-based thermal energy harvesters, Monfray *et al.* describe and test a prototype of thermofluidic harvesting system [24]. The thermofluidic energy harvester operates on a repeating cycle of evaporation and condensation of a working fluid inside a sealed cavity. The temperature of the hot side is above the boiling point of the working fluid, while the temperature of the cold side is below the boiling point of the fluid. This design creates significant pressure within the cavity as the fluid changes between liquid and gaseous states; the pressure change is captured by a piezoelectric membrane and converted into a voltage. Monfray proposes two separate configurations for the thermofluidic energy harvester: a vertical design and a lateral design. The scaling laws described in [2] also govern the output power generated by the thermofluidic energy harvester. In a 2 cm^2 prototype of the vertical design, the authors are able to achieve voltage peaks between 2 and 3 V in steady state. No power density is reported.

The next iteration of the MEMS-based heat energy harvesting concept from Puscasu's research team is a discussion of prototype designs based on the analytical models of the system [3]. The first prototype designs are built, and Puscasu *et al.* discuss the actual results compared with the theoretical potential. Most notably, they indicate the potential for capturing the maximum mechanical energy in the bimetal during its oscillation cycle. Theoretically, the mechanical power density of the snapping bimetal is calculated to be 2.7 mW/cm^2. According to the *k* scaling laws mentioned earlier, a reduction in the device dimensions by a factor of ten would result in a bimetal mechanical power density of 27 mW/cm^2. A power density of 27 mW/cm^2 is orders of magnitude higher than the power density of cutting edge Seebeck thermoelectric

technologies. But real-world efficiency limitations would not allow all of the mechanical energy to be converted to electrical energy.

Boisseau *et al.* discuss the concept of coupling bimetals and electret-based converters to harvest energy from thermal gradients [22]. Bimetal strip technology and electret technology have existed for a while, but combining them for use as a heat engine for energy harvesting purposes is new. Electrets are electrically charged dielectrics able to keep their charge for years, and they enable direct mechanical-to-electrical conversion by acting as a permanent polarization source in electrostatic converters. The use of electrets greatly simplifies the power management required in electrostatic energy harvesting designs. Boisseau states that curved or stamped bimetallic strips are complicated devices that display strong nonlinear behaviors and snap between two stable positions through sudden buckling that is dependent on temperature with a hysteretic behavior. Figure 7 shows the design of the bimetal and electret based converter for thermal energy harvesting.

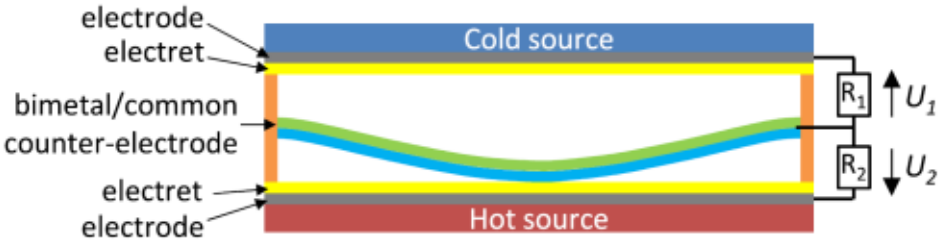

Figure 7. Bimetal and electret based converter for thermal energy harvesting [22]

The design features electret material and electrodes on both the hot source and the cold source such that power can be generated both when the bimetal snaps upward and when the bimetal snaps downward. With the use of an electret surface voltage of 500 V

and a hot side of 60 °C, the mean power output per device is 13.46 µW. The bimetal snapping frequency is 1-3 Hz. The cold side of the device is cooled to 36 °C by forced convection through the use of a fan. The prototype tested in this experiment features a bimetal that is designed to snap at 47 °C and to snap-back at 42.5 °C for a 4.5 °C hysteresis cycle. The authors state that this prototype is non-optimized and suffers from losses in the thermal-to-mechanical energy conversion step. The reported Carnot efficiency is between 0.1% and 0.5%. The device reliability is high.

The next iteration of research on bimetal and electret based thermal energy harvesters by Boisseau seeks to address the efficiency problems identified in his previous publication [25]. In the previous design, without forced convection cooling, a sufficient temperature gradient is unable to be maintained to keep the bimetal oscillating because the thermal control between the two steel layers is not optimized. This limitation is addressed by employing limiting thermal bridges between the two plates. Figure 8 shows the changes made in the design of the bimetal and electret based thermal energy harvester.

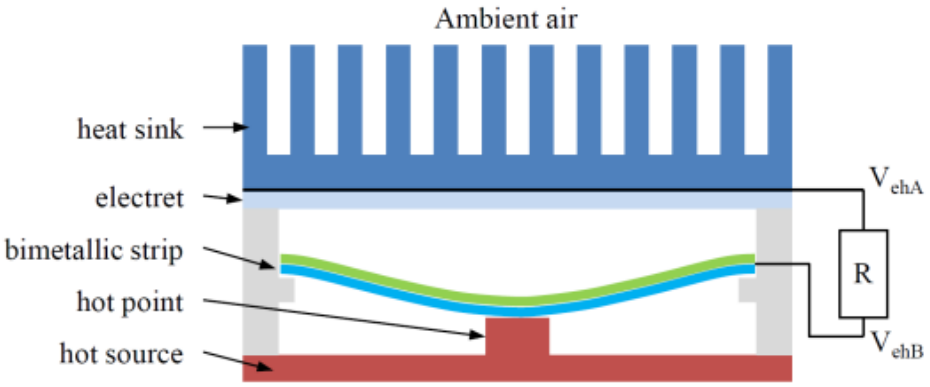

Figure 8. Improved design of bimetal and electret based converter for thermal energy harvesting [25]

The hot point is a small cylinder of copper designed to act as a limiting thermal bridge. Other differences include that a heat sink has been added to the design and a now only one electret material remains on the cold side of the device. Boisseau reports high electromechanical coupling in the improved design. As the surface voltage of the electret increases, the output power of the device increases, but the snapping frequency of the bimetal decreases. However, the generated power of the device ceases to increase for electret surface voltages beyond 600 V. The maximum power attained with the improved design is 5.4 μW per device on a hot source of 70 °C.

Arnaud *et al.* discusses the piezoelectric principles and optimization for the conversion of kinetic energy into electrical energy [26]. The new design modification is that a piezoelectric patch now functions as the electro-mechanical transducer and as the thermal dissipater for the bimetal strip. The piezoelectric patch replaces the need for a heat sink. This optimization raises the harvested energy to 24.6 μJ per snap compared with previous designs that generated 1.8 μJ per snap. Arnaud identifies the benefits of scaling the size of the device down to the micrometer scale. Parasitic capacitances in the larger-sized devices are limiting factors for the efficient operation of a power management circuit. Device down-scaling reduces the impact of these parasitic capacitances. Additionally, the advantages of down-scaling bimetal strips include achieving higher thermal energy transfer rates, higher switching speeds, higher snapping frequencies, and capacitance variations. These advantages lead to overall increased device efficiency and increased power density. Figure 9 shows a graphical display of the stability of Ti-Au bimetal strips versus the bimetal strip thickness for a fixed length of 200 μm.

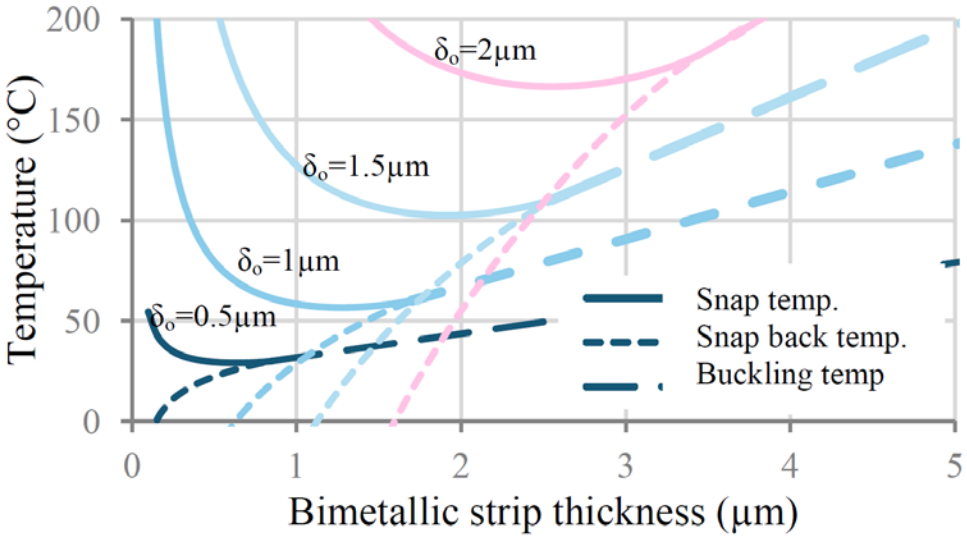

Figure 9. Stability of Ti-Au bimetal strips (L = 200 µm) [26]

δ_o represents the initial curvature of the bimetal. A critical ratio governs the behavior of the bimetal strips: $\delta_o > t / \sqrt{3}$, where t is the total bimetal thickness. If δ_o is less than the ratio, then the snapping quality of the bimetal ceases and only gradual buckling movement occurs. Arnaud also presents a process for producing micro-sized bimetal strips using common fabrication procedures. A photoresist is patterned into arrays of rectangles; the photoresist is then reflowed to produce rounded edges. The two materials that compose the bimetal are deposited; the bimetal materials are patterned and etched. Lastly, the photoresist is removed, and the devices are released.

The next iteration of the research conducted by Puscasu's team concerns a further analysis of the theory that governs the operation of a dual-stage MEMS thermal energy converter [4]. In the article, the authors outline both the thermomechanical conversion laws and the electromechanical conversion laws that apply to the device. The relationships between variables in the equations yield a beneficial result when the

dimensions of the device are scaled down by a factor of *k*. Their analytical findings are summarized below in Table 1.

Table 1. Parameter Evolution from Dimension Down-Scaling [4]

Variable Name	**Effect From Scaling**	**Scaling Factor**
Frequency	↑ Increase	k^2
Snap Temperature	Ø None	Same
Bimetal Force	↓ Decrease	k^2
Piezoelectric and Bimetal Deflection	↓ Decrease	k
Stress and Strain Inside Piezoelectric	Ø None	Same
Piezoelectric Capacitance	↓ Decrease	k
Piezoelectric Voltage	↓ Decrease	k
Transmitted Thermal Power / Surface	↑ Increase	k
Mechanical Power / Surface	↑ Increase	k
Electrical Power / Surface	↑ Increase	k

As denoted in Table 1, the parameters of the thermal harvesting device responded differently to down-scaling the dimensions of the device. It should be noted that there are limits to the increases/decreases of these variables. Infinite heat flux and infinite electrical power are unrealizable objectives. As the dimensions of the device are scaled down, the frequency of the bimetal oscillation increases by a factor of k^2, but the temperature gradient dropped across the device will also decrease due to a higher transmitted thermal power. Therefore, the bimetal oscillation will eventually encounter a limiting factor that prevents continued increase by a factor of k^2. The article concludes by mentioning that the optimal working scale will be determined entirely by the application of the system and the demands of the electrical load.

The latest iteration of research conducted by Puscasu's team describes the actual fabrication of the system and the performed testing on the device [5]. The device is arranged on a flexible Teflon substrate. Harnessing the voltage from the impacted

piezoelectric strip and rectifying the signal yields voltage peaks of up to 16.5 V. The oscillation frequency of the device is 2.4 Hz. With only a 3 K temperature differential, Puscasu reports a power density of 60 $\mu W/cm^3$, which is comparable to most current Seebeck devices. In two-dimensions, the power density for Puscasu's fabricated devices is 0.509 $\mu W/cm^2$. There are still even further advantages of Puscasu's design including device operation in the absence of a heat sink and superior/economical thermal management. Thus, a viable thermal energy harvesting alternative for Seebeck devices is fabricated that displays desirable advantages. However, Puscasu indicates areas of improvement for his work; the device efficiency and cell-to-cell variability needs improvement.

Derivation

An analytical basis for the dual-stage MEMS cantilever energy harvester that is researched in this thesis has been adapted from Lee and is presented in this *Derivation* section [27]. Starting with the mechanical behavior due to strain changes in composite material cantilever actuators, the moment equilibrium condition that governs the deformed shape of a composite beam is as follows:

$$M = -F_1 \frac{t_1 + t_2}{2} \tag{1}$$

where M is the moment acting on the cantilever beam, F_1 is the tensile force acting on the upper layer, t_1 is the thickness of the upper layer, and t_2 is the thickness of the lower layer. The indices "1" and "2" refer to the upper and lower layers of the composite cantilever beam, respectively. The longitudinal stresses of the upper layer and the lower layer are as follows:

$$\sigma_{x1} = \tilde{E}_1 \varepsilon_{x1} = \tilde{E}_1 \frac{\delta_f - \delta_1}{l} = \tilde{E}_1 \left(\varepsilon_f - \varepsilon_1 \right) \tag{2}$$

$$\sigma_{x2} = \tilde{E}_2 \varepsilon_{x2} = \tilde{E}_2 \frac{\delta_f - \delta_2}{l} = \tilde{E}_2 \left(\varepsilon_f - \varepsilon_2 \right) \tag{3}$$

where σ_x is the longitudinal stress, $\tilde{E}$ is the respective Young's Modulus, ε_x is the longitudinal strain, δ_f is the elongation displacement, and l is the beam length. Because of the force equilibrium, it follows that:

$$\sigma_{x1} A_1 + \sigma_{x2} A_2 = 0 \tag{4}$$

where A is the cross-sectional area of its respective layer. By substituting, the strain of the straight beam is written as:

$$\varepsilon_f = \frac{\tilde{E}_1 A_1 \varepsilon_1 + \tilde{E}_2 A_2 \varepsilon_2}{\tilde{E}_1 A_1 + \tilde{E}_2 A_2} \tag{5}$$

using equations (2) and (3). After substituting back into the longitudinal stress equations, the stresses yield:

$$\sigma_{x1} = \tilde{E}_1 \frac{\tilde{E}_2 A_2 \left(\varepsilon_2 - \varepsilon_1 \right)}{\tilde{E}_1 A_1 + \tilde{E}_2 A_2} \tag{6}$$

$$\sigma_{x2} = -\tilde{E}_2 \frac{\tilde{E}_1 A_1 \left(\varepsilon_2 - \varepsilon_1 \right)}{\tilde{E}_1 A_1 + \tilde{E}_2 A_2} \tag{7}$$

using equation (5). The relative strain is defined as:

$$\varepsilon = \frac{\delta_2 - \delta_1}{l} = \varepsilon_2 - \varepsilon_1 \tag{8}$$

and three ratios of the geometric/material properties between the two layers are defined as:

$$p = \frac{t_1}{t_2}, q = \frac{w_1}{w_2}, r = \frac{\tilde{E}_1}{\tilde{E}_2} \tag{9}$$

to aid the management of terms in the derivation. Using the three newly defined equations in (9), the stress equations can be written as:

$$\sigma_{x1} = \tilde{E}_2 \frac{r\varepsilon}{1+pqr} \tag{10}$$

$$\sigma_{x2} = -\tilde{E}_2 \frac{pqr\varepsilon}{1+pqr} \tag{11}$$

by substitution. The moment condition is applied, and the moment equation is solved as:

$$M = \frac{1}{2}\sigma_{x2} w_2 t_2^{\,2}\left(1+p\right) = -M_{eff} \tag{12}$$

where M_{eff} is the effective moment. The resulting radius of curvature from the deflecting beam is as follows:

$$\rho = \frac{\left(\tilde{E}I\right)_{eff}}{M_{eff}} = \frac{t_2}{6\varepsilon}\frac{3\left(1+p\right)^2 + \left(1+pqr\right)\left(p^2 + 1/\,pqr\right)}{1+p} \tag{13}$$

where ρ is the radius of curvature, and $(\tilde{E}I)_{eff}$ is the effective flexural rigidity. The radius of curvature is written as:

$$\rho = \frac{t}{2\varepsilon}\left[1 + \frac{1+pqr}{3\left(1+p\right)^2}\left(p^2 + \frac{1}{pqr}\right)\right] \tag{14}$$

after simplifying. The relative strain can be written as:

$$\varepsilon = \frac{\delta_2 - \delta_1}{l} = \frac{d_{31}}{t_1}V \tag{15}$$

$$\varepsilon = \frac{1+p}{p}\frac{d_{31}}{t_1}V \tag{16}$$

where d_{31} is the bending charge constant, and V is the voltage. By substituting into equation (14), the new radius of curvature is:

$$\rho = \frac{t^2}{2d_{31}V}\frac{p}{1+p}\left[1+\frac{1+pqr}{3(1+p)^2}\left(p^2+\frac{1}{pqr}\right)\right] \tag{17}$$

with a maximum deflection of:

$$y_l = \frac{l^2}{2\rho} = \frac{1+p}{p\left[1+\frac{1+pqr}{3(1+p)^2}\left(p^2+\frac{1}{pqr}\right)\right]}\left(\frac{l}{t}\right)^2 d_{31}V \tag{18}$$

where y_l is the vertical deflection. Further substitution for the relative strain yields:

$$\varepsilon = \frac{\delta_2-\delta_1}{l} = (\alpha_2-\alpha_1)(T_H-T_C) \tag{19}$$

where α is the respective coefficient of thermal expansion, and T_H and T_C are the temperatures of the hot side and cold side, respectively. By substituting into equation (14), the next radius of curvature is:

$$\rho = \frac{t}{2(\alpha_2-\alpha_1)(T_H-T_C)}\left[1+\frac{1+pqr}{3(1+p)^2}\left(p^2+\frac{1}{pqr}\right)\right] \tag{20}$$

with a maximum vertical deflection of:

$$y_l = \frac{l^2}{2\rho} = \frac{l^2(\alpha_2-\alpha_1)(T_H-T_C)}{t\left[1+\frac{1+pqr}{3(1+p)^2}\left(p^2+\frac{1}{pqr}\right)\right]} \tag{21}$$

after substituting. By setting equations (18) and (21) equal to each other, the relationship between voltage and thickness can be determined:

$$V = \frac{1}{2}\frac{(\alpha_2 - \alpha_1)(T_H - T_C)t}{d_{31}} \sim \frac{1}{k} \tag{22}$$

to predict the effect of bimetal thickness scaling. This relationship agrees with Puscasu's research by predicting a decrease in output voltage by a factor of *k* when the cantilever beam's dimensions are scaled down by a factor of *k*. This claim agrees with the derivations found in Puscasu's research.

To determine the scaling relationship between the cantilever dimensions and the operational frequency, the heat transfer characteristics are described by the one-dimensional heat conduction equation:

$$\frac{d^2T}{dx^2} = -\frac{\dot{Q}_t}{k_s A} \tag{23}$$

where T is the temperature, x is the axis defined along the length of the cantilever, $\dot{Q}_t$ is the generated heat, k_s is the thermal conductivity, and A is the cross-sectional area. This equation can be solved using the boundary conditions T_C at $x = 0$ and T_H at $x = l$ to give the following temperature equation:

$$T = \frac{\dot{Q}_t l^2}{2k_s A}\left[\frac{x}{l} - \left(\frac{x}{l}\right)^2\right] + (T_H - T_C)\frac{x}{l} + T_C \tag{24}$$

where T_H and T_C are the respective hot and cold temperatures, and l is the cantilever beam length. Adapting the equation to model a cantilever beam with one fixed end, the boundary conditions $T = T_C$ at $x = 0$ and $dT/dx = 0$ at $x = l$ results in:

$$T = \frac{\dot{Q}_t l^2}{2k_s A}\left[2\frac{x}{l} - \left(\frac{x}{l}\right)^2\right] + T_C \tag{25}$$

to find the temperature along the beam. One simplification to find the temperature at $x = l$ yields:

$$T_H = \frac{\dot{Q}_t l^2}{2k_s A} + T_C \tag{26}$$

after substituting. With the equation in this form, the scaling relationship between the cantilever dimensions and time becomes evident. $\dot{Q}_t$ is defined as the heat generated per unit beam length per unit time. Therefore, similar *k*-factor logic from the analytical derivations featured in [2, 4] explains the effect of dimensional scaling as it relates to the cantilever beam oscillation frequency and ultimately the electrical power output. Noting the relationship between $\dot{Q}_t$ and l^2 in equation (26), time is directly proportional to the square of the length:

$$t \sim l^2 \tag{27}$$

which implies that the frequency is directly proportional to the inverse of the square of the length:

$$f \sim \frac{1}{l^2} \sim k^2 \tag{28}$$

predicting that a reduction in device dimensions by a factor of *k* would increase the cantilever beam oscillation frequency by a factor of k^2. This claim agrees with the derivations found in Puscasu's research. The electrical energy produced by the piezoelectric material is defined as:

$$E_{el} = \frac{1}{2} C_p V^2 \tag{29}$$

where E_{el} is the electrical energy, C_p is the capacitance, and V is the generated voltage. To account for the increased number of devices inherent in the k-factor scaling construct, the number of devices relates as:

$$\sqrt{N_s} \sim k \tag{30}$$

where N_s is the unit-less total number of devices. Finally, the total electrical power is derived by combining equations (28), (29), and (30):

$$P_{eltot} = N_s E_{el} f \sim k \tag{31}$$

where P_{eltot} is the total electrical power generated by N_s number of devices. While maintaining a fixed total area, the total electrical power ultimately increases by a factor of k when the device dimensions are scaled down by a factor of k. This claim also agrees with the analytical derivations found in [2, 4].

Summary

A summary of the previously conducted research and necessary future research in the subfield of non-Seebeck thermal energy harvesting methods is as follows. As with all aspects of the thermal energy harvesting field, improving device power density is a key objective [1]. Additionally for non-Seebeck thermal energy harvesters, efficiency becomes another key area of improvement. Puscasu *et al.* state that one of the major needs for future research on dual-stage thermal MEMS energy converters is the energy conversion efficiency [5]. The design of these converters inherently involves two stages of energy conversion, which allows the opportunity for losses to occur in each energy

transition process. The authors identify that a snapping bimetal that absorbs its own kinetic energy will induce losses in the thermal to mechanical energy conversion. The authors also identify that the mechanical to electrical energy conversion efficiency is on the order of a few percent because only the forward snap energy is captured by the piezoelectric transducer. Bimetals that do not absorb their own kinetic energy and piezoelectric transducers that have low mechanical damping and high coupling factors will address these efficiency obstacles. Especially in forms of low-power applications, efficiency is paramount since voltage and current magnitudes are already small.

Energy harvesting applications that involve the human body are low power also and generate milliwatt-size signals according to current technology [23]. Future research for thermal energy harvesting applied to the human body requires device miniaturization because wearable devices must be both ergonomic and unobtrusive in nature. Non-Seebeck devices offer a viable solution to this requirement because they show increasing promise for out-performing the semiconductor-based thermal energy harvesters without the use of a heat sink.

Table 2 shows a summary of the key parameters for the research presented in this literature review.

Table 2. Summarized list of performance metrics for the surveyed energy harvesters

Author	Year	Device Type	Device Dimensions	Voltage	Power Density
Xie [9]	2014	Piezoelectric	0.2/0.4 m × 1 m × 1 m		12.7 W
Lin [10]	2013	Electrostatic	2 mm × 2 mm × 0.03 mm	15 V	2.5 μW
Arakawa [12]	2004	Electrostatic	20 mm × 20 mm × 2 mm	200 V	7.5 $\mu W/cm^3$
Shenck [13]	2001	Piezoelectric			8.4 mW
Varadrajan [15]	2013	Piezoelectric	6 cm × 3 cm × 0.1 cm	0.1166 V	0.18 $\mu W/cm^2$
Boisseau [16]	2011	Electrostatic	30 mm × 13 mm × 0.3 mm		12.82 $\mu W/cm^2$
Böttner [17, 18]	2004	Seebeck Thermoelectric	20 μm × 40 μm × 80 μm		60 $\mu W/cm^2$
Glosch [19]	1999	Seebeck Thermoelectric	500 μm × 7 μm × 1.2 μm	0.4 V	0.2 μW
Venkatasubramanian [20]	2001	Seebeck Thermoelectric		0.042 V	6.1 mW/cm^2
Dalola [21]	2008	Seebeck Thermoelectric		0.9 V	0.9 mW
Leonov [23]	2013	Seebeck Thermoelectric	3 cm × 3 cm × 5 mm		1-4 mW
Monfray [24]	2012	Non-Seebeck Thermoelectric	2 cm^2	2-3 V	
Puscasu [3]	2012	Non-Seebeck Thermoelectric	36 mm × 18 mm × 0.2 mm	10 V	0.772 $\mu W/cm^2$
Boisseau [22]	2013	Non-Seebeck Thermoelectric	34 mm × 12 mm × 1.5 mm	>400 V	22 $\mu W/cm^3$
Boisseau [25]	2013	Non-Seebeck Thermoelectric	20 mm × 10 mm × 0.115 mm	>600 V	6.4 μW
Puscasu [5]	2014	Non-Seebeck Thermoelectric	36 mm × 18 mm × 3.8 mm	16.5 V	0.509 $\mu W/cm^2$

New novel methods in energy harvesting for capturing energy are constantly being presented and challenging the previously established limitations. The next chapter will discuss the adopted methodology for this thesis research.

III. Methodology

Chapter Overview

The methodology of this experimentation is designed to observe the effect of bimetal thickness scaling and test the performance of the cantilever design of the dual-stage MEMS cantilever energy harvester. The remaining sections of this chapter describe the system boundaries within the simulation environment, the pertinent variables that govern the operation and performance of the dual-stage MEMS cantilever energy harvester, the campaign of experiments, and methods for analyzing the results of the simulations.

Experiment Design

a. Design Overview

Using the bimetal and piezoelectric based harvester from the literature as a starting point, a cantilever-based design is proposed in this research [5]. The dual-stage MEMS cantilever energy harvester is a beam design composed of three layers. The bottom active layer is aluminum; the middle passive layer is SiO_2; the top piezoelectric layer is PZT-5H. One major difference in the design configuration of dual-stage MEMS cantilever energy harvester when compared with the bimetal and piezoelectric based harvester from the literature is that the design is not impact-based. The aspect of transferring mechanical energy to the piezoelectric material through impact is removed to improve the energy conversion efficiency of the piezoelectric material. The output energy of piezoelectric ceramics is orders of magnitude larger when achieved through gradual stress as opposed to impact stress [28]. Therefore, one intended advantage to

depositing the piezoelectric material directly on the bimetal is to gain the benefits of using a gradual stress design instead of using an impact stress design. The fixed end of the beam is the cold side of the device. The free end of the beam makes contact with the hot side of the device. The dual-stage MEMS cantilever energy harvester operates by heating up while it remains in contact with the hot side; the change in temperature induces a mechanical stressing response in the cantilever beam due to the bimetal characteristics. The mechanical stressing response of the cantilever beam generates a voltage potential on the piezoelectric material. Therefore, the device is dual-stage because it first converts thermal energy into mechanical energy and then converts mechanical energy into electrical energy.

b. Objectives

The objective of the experimentation is to compare the performance of the dual-stage MEMS cantilever energy harvester in simulation as the thickness parameter is altered over one order of magnitude. The performance of the dual-stage MEMS cantilever energy harvester will also be compared with the performance of Seebeck devices as well as the bimetal and piezoelectric based harvester from the literature [5]. An increase or decrease in performance will be determined by the change in the identified response variables.

c. System Boundaries

The chosen simulation environment for this research is COMSOL® Multiphysics. Using this software, the user is able to define the system boundaries that govern the physics which determine the operation of the device. Users create COMSOL® models in the Model Builder window, which contains all definitions that describe the simulated

system. The thickness scaling for the dual-stage MEMS cantilever energy harvester design is tested in two dimensions. Though the design will be modeled in 2D, COMSOL® allows the user to enter the thickness of the design to account for the third dimension. Therefore, the power density in units of W/cm^2 is able to be extracted from the simulation results due to the thickness consideration.

Figure 10 shows the two-dimensional design layout and the material assignment for each domain.

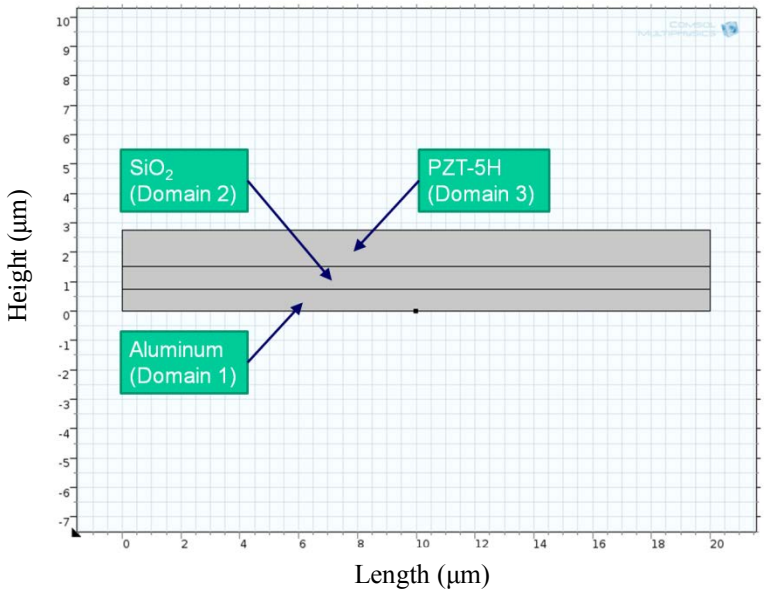

Figure 10. 2D layout of dual-stage MEMS cantilever energy harvester design

The two-dimensional model functions as a cross-sectional slice of the device and is built under the Geometry node in COMSOL®. The design consists of a single geometry composed by the union of three domains. The lower domain (domain 1), middle domain (domain 2), and upper domain (domain 3) represent the active layer, the passive layer, and the piezoelectric material, respectively. Each domain is assigned a material under the Materials node. The active layer is composed of Aluminum, which

has a CTE of 23e-6 K^{-1}. The passive layer is composed of silicon dioxide, which has a CTE of 0.5e-6 K^{-1}. Therefore, the CTE of the two bimetal materials differ by a factor of 46. PZT-5H was chosen as the piezoelectric material. PZT-5H is very similar in material properties to the more common PZT-5A, but it has higher sensitivity and permittivity than PZT-5A [29]. One drawback of PZT-5H is a limited temperature working range, but for the temperature applications presented in this research, this drawback is avoided.

Figure 11 shows the important boundary definitions that govern the operational characteristics of the device.

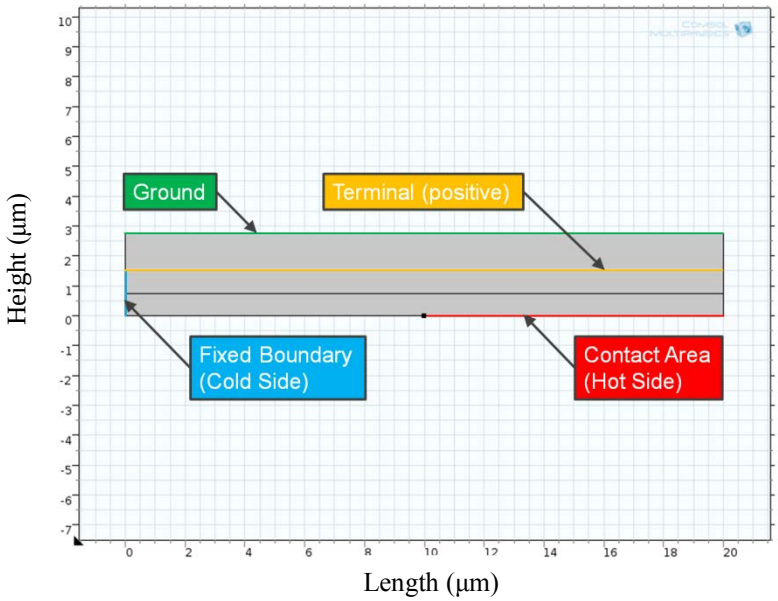

Figure 11. Boundary definitions of the dual-stage MEMS cantilever energy harvester

The leftmost boundary of the bimetal is designated a fixed boundary to model the presence of the cantilever beam's anchor. The cantilever's anchor is also modeled as the cold side of the device, where the heat in the arm of the cantilever escapes once the cantilever comes out of contact with the hot side. The 10 µm boundary section on the underside of the active layer is designated as the hot side. The hot side is modeled as a

temperature boundary and is fed a heat input function that brings the boundary to the temperature of the hot side briefly, which is representing the time that the cantilever beam would be in contact with the hot side. The topmost boundary is designated as ground and represents the grounded terminal of the piezoelectric material. The bottom boundary of the piezoelectric material is designated terminal, which is where the boundary probes read the voltage signal generated by the piezoelectric material.

The setup requires three physics packages solved simultaneously to compute the solution. The first employed physics package is Piezoelectric Devices. Each fixed constraint and terminal assignment is listed under the Piezoelectric Devices node. Domain 3 is designated as the piezoelectric material, which is orientated in the Material XZ-Plane coordinate system. Domains 1-3 are specified as Linear Elastic Material. As a subset of the Linear Elastic Material subnode, the bimetal is given a Thermal Expansion. Thermal Expansion allows the user to set the strain reference temperature and apply model input temperatures to the bimetal domains. The strain reference temperature describes the temperature where there are zero stresses or strains in a material; for this research, the strain reference temperature is set to the temperature of the cold side at 296.15 K. The model input temperature is set as an iteratively tuned piecewise function that represents the transfer of heat between domains once they make contact. The Fixed Constraint is applied to the leftmost boundaries of the bimetal to model the presence of the anchor. The upper boundary of the piezoelectric material is designated a Ground node, while the lower boundary of the piezoelectric material is designated a Terminal node to extract the electrical response of the PZT-5H.

The second employed physics package is Heat Transfer in Solids. This package models the thermal characteristics of the bimetal. A Temperature node designates the leftmost boundary of the bimetal as the temperature of the cold side at 296.15 K. Another Temperature node designates the contact boundary on the bimetal as the heat input function that models the latching operation of the dual-stage MEMS cantilever energy harvester.

The third employed physics package is Electrical Circuit. This package uses the Ground and Terminal nodes under the Piezoelectric Devices package to form a virtual circuit. The output circuit is composed of a 1 kΩ resistor acting as the load. A 1 kΩ resistor is chosen to avoid the difficulties described in the literature review where energy harvesting devices suffer losses in output power from parasitic capacitances. Parasitic capacitances have been linked with high-resistance loads and must be accounted for in the design of the energy harvesting system [16]. It is understood that a real-world implementation of the dual-stage MEMS cantilever energy harvester would need to be impedance matched to the particular biomedical sensor or electronic device for which the energy harvester provides power.

The Mesh node describes the how each domain is partitioned into finite elements. The device components are meshed using a Mapped Distribution. A total of 100 boundary elements are mapped along the lower boundary of the bimetal. 2 boundary elements are mapped along the rightmost edge of the bimetal; 2 boundary elements are mapped along the rightmost edge of the piezoelectric material. Therefore, the complete mesh consists of 400 domain elements.

The employed solver is a Time-Dependent study. A backward differential (BDF) solver is chosen with an intermediate time-stepping method. The Direct solver is enabled, and the Fully Coupled subnode is added to the study. The Fully Coupled subnode forces the solver to simultaneously evaluate all three physics packages at the same time rather than independently.

d. Assumptions and Limitations

Simulations often suffer from limitations in their ability to exactly predict real-world operation of models. This subsection discusses the assumptions and limitations present in this body of research and their effect on a real-world implementation of the dual-stage MEMS cantilever energy harvester.

One key characteristic that makes the operation of the dual-stage MEMS cantilever energy harvester effective is that the cantilever arm must remain in contact with the hot side of the device to heat the active layer enough before the beam deflects. This concept is referred to as latching. Latching involves holding the beam against the hot side with an external force to allow significant transfer of heat. Within the simulation, this effect is achieved by the heat input function that applies the temperature of the hot side to the contact area for a brief amount of time, which is tuned to return the highest peak voltage out of the device. In a real-world implementation, this effect could be achieved in a number of ways. The first proposed method is to employ permanent magnets to hold the tip of the cantilever beam down long enough to heat. This system requires no external circuitry, but accommodations would have to be made for additional weight and heat transfer effects. Employing permanent magnets takes advantage of the characteristics of magnetic forces that drop off with $1/r^2$ (with distance r) in the near field

and with $1/r^3$ (with distance r) in the far field. Therefore, the attractive force between the cantilever beam tip and the hot side would be greatest when the two objects were in contact and weakest when the cantilever beam reached maximum deflection. One challenge that employing permanent magnets encounters is that current wafer-scale fabrication techniques are not suited for depositing and patterning magnetic materials [1]. The second proposed method is to electrostatically maintain contact between the cantilever beam tip and the hot side. This system does require external circuitry, but no accommodations for additional weight or heat transfer effects would be necessary. A voltage pad with an accompanying dielectric layer would be deposited underneath the cantilever beam, but not interfering with the hot side. The voltage would be set at a constant negative voltage to take advantage of the characteristics of electrostatic forces that drop off with $1/r^2$ (with distance r). Therefore, the attractive force between the cantilever beam and the voltage pad would be greatest when the cantilever experienced zero deflection and weakest when the cantilever beam reached maximum deflection. One variation on this method is to use a square wave as the signal on the voltage pad that is synced with the frequency of the cantilever beam's displacement cycle. In both variations, the only power consumption suffered is leakage losses in the external circuitry because there is no closed circuit in these two proposed methods. The signals on the voltage pad could be generated from the electrical output of the dual-stage MEMS cantilever energy harvester. From the use of output-generated voltage signals, there would be a transitory period of reduced efficiency until the device reached full efficiency at steady state. The third proposed method is to use an electret material to latch the cantilever beam. Electrets are stable electrically charged dielectrics that are capable of

holding their charge for many years (high reliability). This system requires no external circuitry, and no accommodations have to be made for additional weight or heat transfer effects; thus, it is the most desirable latching technique. The voltage would be set at a constant negative voltage to take advantage of the characteristics of electrostatic forces that drop off with $1/r^2$ (with distance r). Therefore, the attractive force between the cantilever beam and the voltage pad would be greatest when the cantilever experienced zero deflection and weakest when the cantilever beam reached maximum deflection.

The contact area, as defined in the simulation, is where the underside of the cantilever beam and the hot side of the device overlap. The contact area used for this research is a 10 μm × 10 μm square. In real-world MEMS devices, stiction can become an issue for large contact areas. Stiction can be avoided through material choice and the use of dimples in the design. A real-world implementation of the dual-stage MEMS cantilever energy harvester might use gold on the top surface of the hot side and place dimples on the underside of the cantilever beam's contact area to ensure that stiction does not prevent the device from operating. The use of gold improves the reliability of the device over time, and the dimples minimize the surface area shared between the two objects in contact to mitigate the possibility of the objects becoming stuck together by surface adhesion forces.

Another assumption that is crucial to the design of the dual-stage MEMS cantilever energy harvester is that the cantilever beam must be thermally isolated from the hot side of the device with the exception of the contact area. If the substrate is to be considered the hot side of the device, then the cantilever beam must be anchored to a thermally insulating layer that separates the cantilever from the substrate. Thermal

isolation is paramount because the cantilever is modeled as the cold side of the device. Therefore, heat transfer between the hot side and cold side of the device that does not contribute to the mechanical deflection of the beam degrades the efficiency.

e. Identified Variables

Variables for three dimensions are identified and included in this section. The primary response variable is the power density. The electrical power density is commonly measured in Watts per square centimeter (W/cm^2) for energy harvesting devices and is the most important performance metric in this thermal energy harvesting system. The ultimate goal of an effective modular energy harvesting system is the maximization of the electrical power density because the devices must not deliver maximum power only; they must deliver maximum power while also using space efficiently. Variables of lesser importance that function as response variables are the bimetal oscillation frequency, mechanical force developed, beam deflection, voltage, transmitted thermal power density, and mechanical power density. These response variables result from the control variable inputs and determine a system response for the device.

The control variables of interest in this body of research are the thickness of the bimetal and the heating interval of the contact area. The length and width of the beam are fixed at 20 μm and 10 μm, respectively. The bimetal thickness is scaled over one order of magnitude from 10 μm down to 1 μm to affect the response variables. The employed materials in the device are chosen as aluminum, silicon dioxide, and PZT-5H. Excluding the parts not built in the simulation, in its most basic form, the design of the dual-stage MEMS cantilever energy harvester consists of three unique materials to achieve the

thermal, mechanical, and electrical characteristics that enable an energy harvesting system. These three materials are easily interchangeable in the simulation environment by entering the applicable material properties. The mentioned control variables and the specific levels associated with each are listed in Table 3.

The most notable constant in this body of research is the temperature gradient, which will be held constant at a 10 °C differential between the temperatures 33 °C (human skin) and 23 °C (ambient air). Additional constants include the length and width of the cantilever and the materials used in the simulation. The variables are summarized in Table 3 below.

Table 3. Variable Summary

Response Variables	Power Density ($\mu W/cm^2$)	Peak Voltage (V)	Frequency (Hz)
Control Variables	Factors	Geometry (mm)	Heat Input Function (K)
	Levels	Bimetal Thickness (1x – 0.1x)	Latching Time (0.09 μs – 0.15 μs)
Constants	Hot Side Temperature (33 °C)		Cold Side Temperature (23 °C)
	20 μm Cantilever Beam Length		10 μm Cantilever Beam Width
	100 μm^2 Contact Area		1 kΩ Resistive Load

f. Data Analysis and Interpretation

COMSOL® is a deterministic software, meaning that for one particular unique and adequate set of inputs, COMSOL® will return the same unique and identical output every single time the user runs the simulation. A deterministic output that has no variance severely limits any statistical analysis, but the main goal of this research is to compare the device performance through varying the control variables to find a superior design that

competes with Seebeck performance and with the performance of non-Seebeck devices from the literature [5].

The compiled test matrix provided in Table 4 describes the campaign of experiments that is expected to satisfy the research objectives.

Table 4. Test Matrix

Test	**Control Variables**		**Response Variables**		
	Bimetal Thickness	Heat Input Function	Power Density	Peak Voltage	Bimetal Oscillation Frequency
1	1 × Thickness	0.09 μs – 0.15 μs	Power Density	Peak Voltage	Bimetal Oscillation Frequency
2	0.75 × Thickness	0.09 μs – 0.15 μs	Power Density	Peak Voltage	Bimetal Oscillation Frequency
3	0.5 × Thickness	0.09 μs – 0.15 μs	Power Density	Peak Voltage	Bimetal Oscillation Frequency
4	0.45 × Thickness	0.09 μs – 0.15 μs	Power Density	Peak Voltage	Bimetal Oscillation Frequency
5	0.4 × Thickness	0.09 μs – 0.15 μs	Power Density	Peak Voltage	Bimetal Oscillation Frequency
6	0.35 × Thickness	0.09 μs – 0.15 μs	Power Density	Peak Voltage	Bimetal Oscillation Frequency
7	0.3 × Thickness	0.09 μs – 0.15 μs	Power Density	Peak Voltage	Bimetal Oscillation Frequency
8	0.25 × Thickness	0.09 μs – 0.15 μs	Power Density	Peak Voltage	Bimetal Oscillation Frequency
9	0.2 × Thickness	0.09 μs – 0.15 μs	Power Density	Peak Voltage	Bimetal Oscillation Frequency
10	0.15 × Thickness	0.09 μs – 0.15 μs	Power Density	Peak Voltage	Bimetal Oscillation Frequency
11	0.125 × Thickness	0.09 μs – 0.15 μs	Power Density	Peak Voltage	Bimetal Oscillation Frequency
12	0.1 × Thickness	0.09 μs – 0.15 μs	Power Density	Peak Voltage	Bimetal Oscillation Frequency

As featured in the test matrix, the thickness scaling has been designed to cover one order of magnitude as a means of determining the extent to which the analytical model holds true over a wide range. For all cases, the power density, peak voltage, and bimetal oscillation frequency are the most desired response variables. Therefore, each response variable can be plotted against the bimetal thickness to determine the relationship.

For all response variables, the simulation results are expected to follow the analytical models that are outlined in the literature [2, 3, 4, 5]. Although analytical derivation and simulation are both abstract approaches to modeling the dual-stage MEMS

cantilever energy harvester, they will undoubtedly produce different power density results because the former is a theoretical method while the latter is a numerical method.

Summary

An approach for determining the effects of device miniaturization through bimetal thickness scaling has been presented. The next section will discuss the results of the research.

IV. Analysis and Results

Chapter Overview

This section presents the results of the 2D simulations of the dual-stage MEMS thermal energy harvester. Experimentation in this research addresses aspects of varying the control variable: bimetal thickness. The simulation process determines how the control variable affects the response variables and is recorded in this chapter. The campaign of experiments described in the test matrix from the *Methodology* chapter yields the following results.

Larger Bimetal Thicknesses

From the test matrix in Table 4, the bimetal thickness scaling ranges one order of magnitude from 10 μm down to 1 μm. Each tested cantilever beam responds similarly when in contact with the hot surface by curling upwards as a result of the expanding active bimetal layer. The results from the 5 μm bimetal thickness simulation are presented below to explain the behavior of the cantilever beam at larger bimetal thicknesses. Figure 12 shows the contact area of the 5 μm thick bimetal cantilever as it is heated by the hot surface.

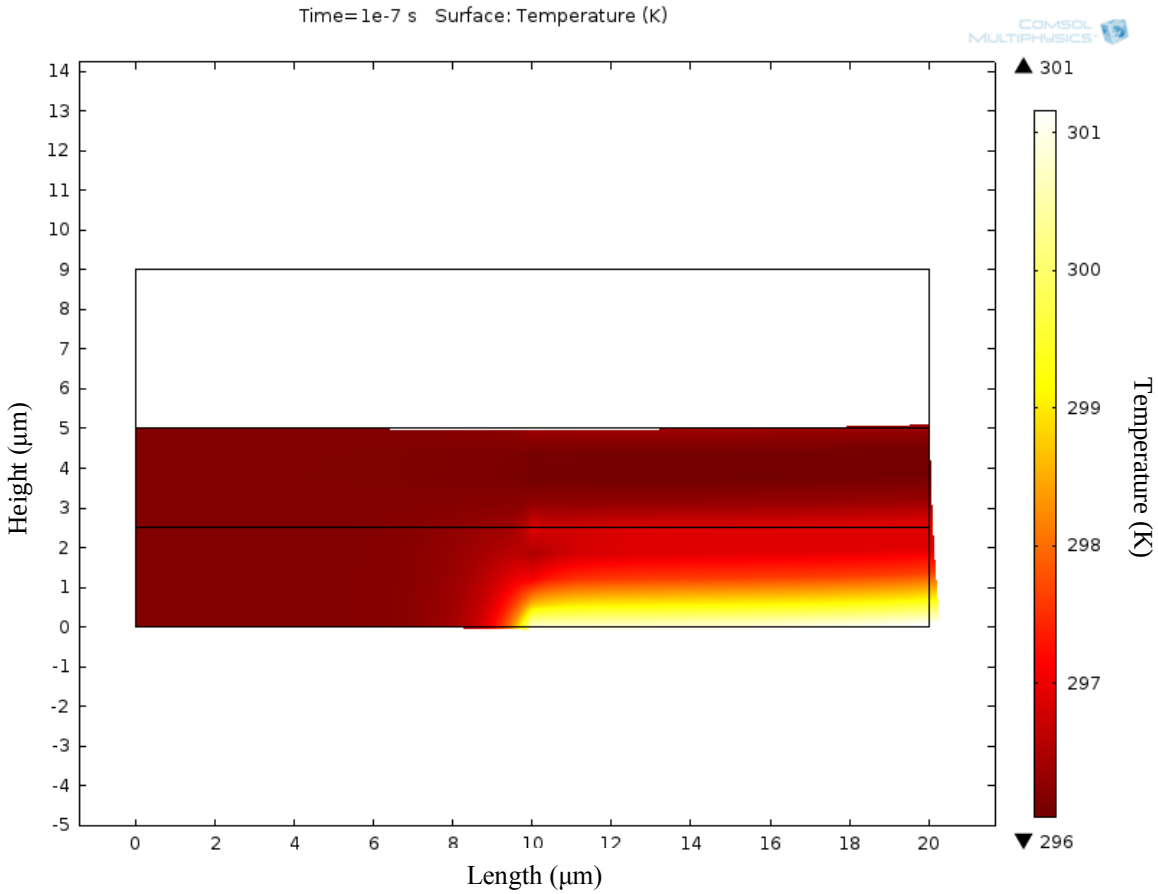

Figure 12. Expanding active bimetal layer (deformation scale 500; PZT layer not shown)

While contact between the cantilever beam and the hot surface is maintained, the active bimetal layer expansion creates internal stress in the cantilever beam, which causes the curling effect. Figure 13 shows the tip displacement of the cantilever beam for the 5 µm thick bimetal.

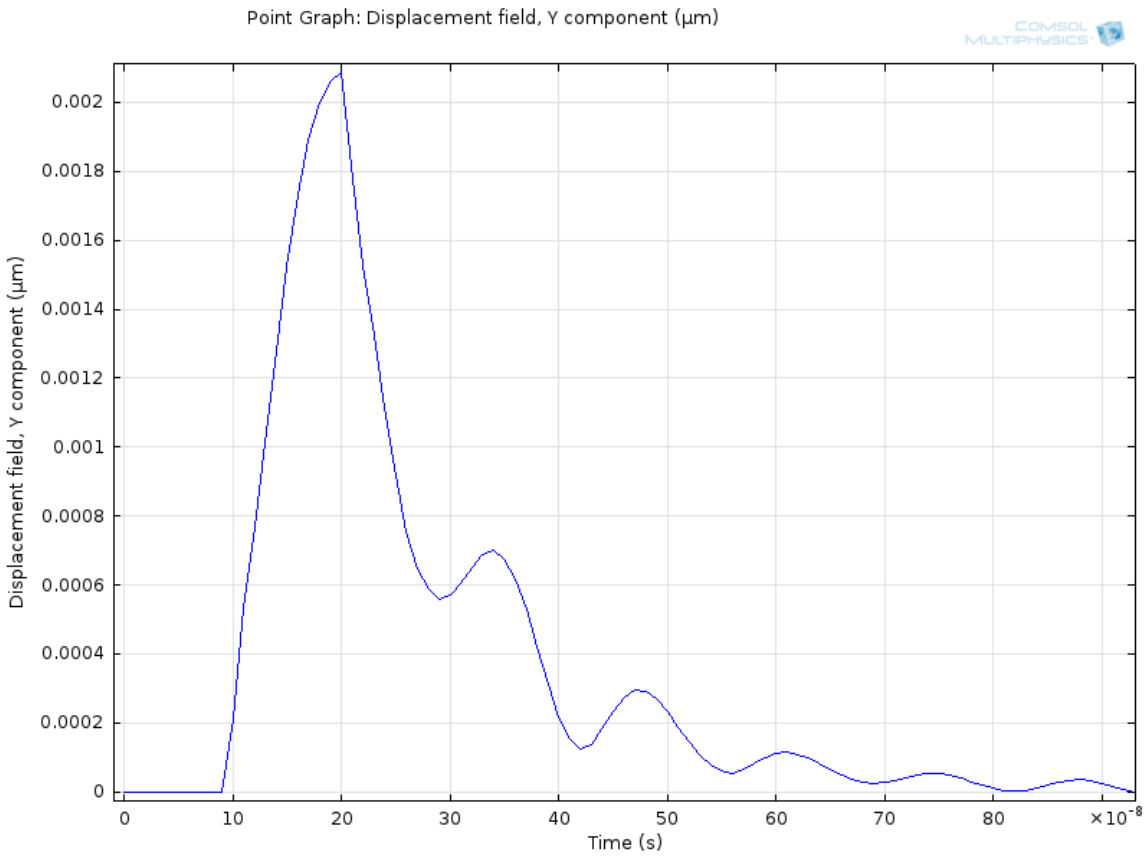

Figure 13. 5 µm thick bimetal cantilever tip displacement

Cantilever beams at larger thicknesses display a displacement behavior consistent with the 5 µm thick bimetal simulation. At first, there is a large displacement peak in response to the temperature change at the contact area. Then, as the beam cools, the cantilever beam's resonant frequency influences the tip displacement through an

underdamped response until the displacement reaches zero again. The displacement cycle repeats once the bimetal comes in contact with the hot surface after cooling.

The produced voltage from the piezoelectric material correlates with the cantilever tip displacement shown in Figure 13. The peaks and troughs in the voltage signal reflect the underdamped displacement response of the cantilever beam. Each conducted simulation is individually tuned to maximize the peak voltage from the piezoelectric material. Figure 14 shows the voltage recorded by Boundary Probe 1 in the 5 μm bimetal thickness simulation.

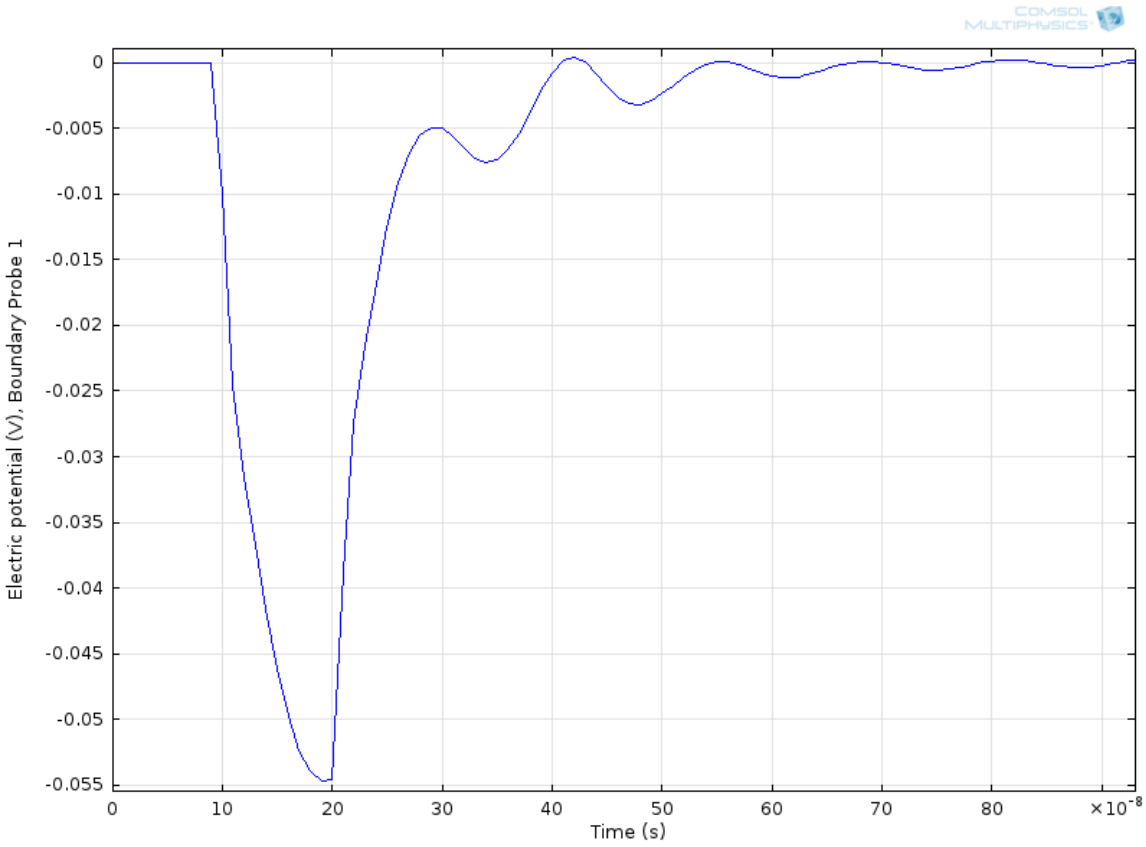

Figure 14. 5 μm thick bimetal cantilever voltage signal

The tuning process for each simulation involves finding the "roll-off" point of the produced voltage. This process is governed by the length of the heating time, which represents the length of time that the cantilever beam is forced to remain in contact with the hot surface before release. As seen in Figure 14, the voltage signal reaches its maximum just before the cantilever tip displacement reaches its maximum in Figure 13. This is the desired effect that identifies the "roll-off" point. Boundary Probe 1 is set to record the voltage on the underside of the piezoelectric material. The coordinate system selection for the piezoelectric material orientation in the simulation is set to the *XZ*-plane, which yields a negative voltage when the bottom face of the piezoelectric material is subject to tensile stress. Figure 15 shows a surface plot of the electric potential through one vertical slice of the 5 μm bimetal thickness cantilever beam as it is stressed.

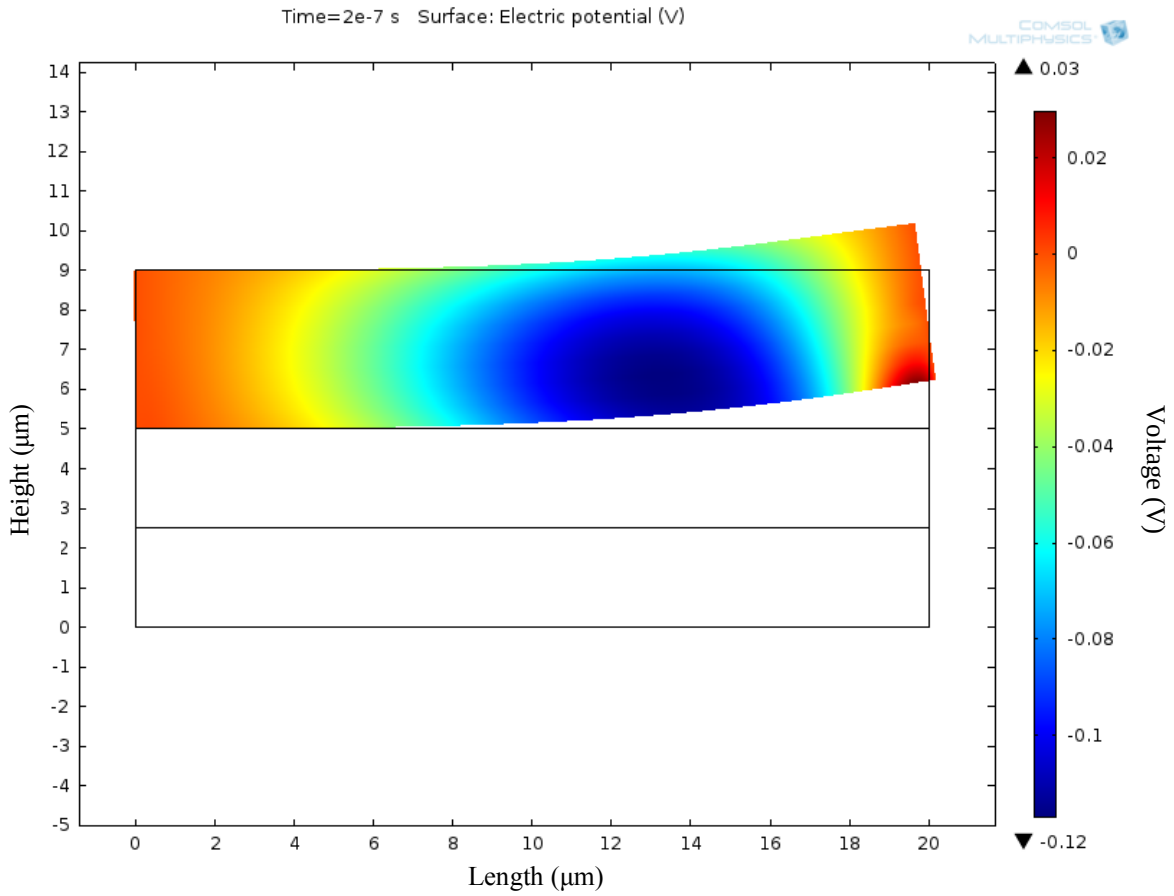

Figure 15. Stressed piezoelectric material (deformation scale 500; bimetal layer not shown)

The largest voltage magnitude resides at the location where the piezoelectric material experiences the most bending. Figure 15 is showing the state of the piezoelectric material at 0.2 μs, which is where the maximum voltage magnitude occurs in Figure 14. As can be noted from the color legend, the largest voltage magnitude is in the dark blue area at -0.12 V. However, in Figure 14, -0.12 V is not the maximum voltage magnitude recorded in the voltage signal. This is because the simulation treats the entire lower boundary of the piezoelectric material as a conductor and therefore

averages across the boundary to produce a net voltage. The net voltage value is then dropped across the 1 kΩ resistor through the virtual circuit.

The current density also correlates with the features described in the cantilever tip displacement plot in Figure 13. It is expected that the beam tip displacement would strongly influence the voltage signal and the current density produced by the piezoelectric material because the output of the piezoelectric material depends on its mechanical input. Figure 16 shows the current density of the piezoelectric material in the 5 μm bimetal thickness simulation.

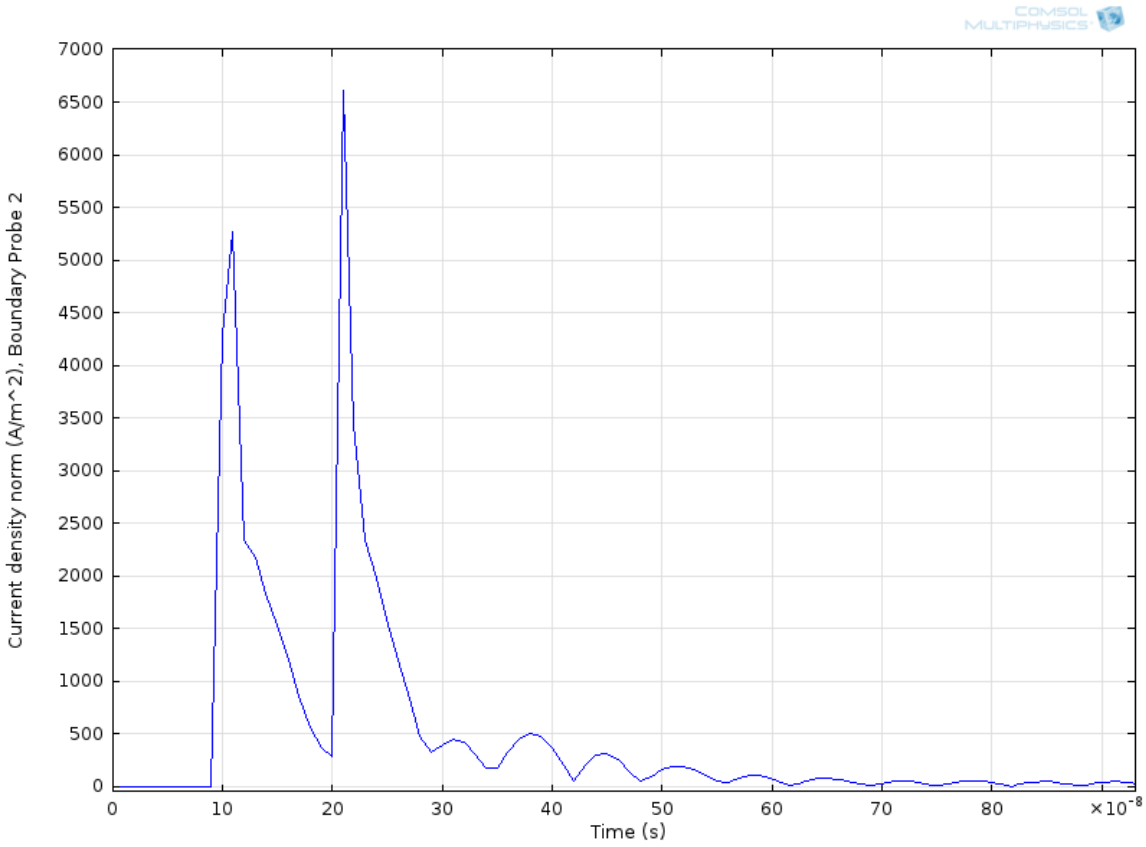

Figure 16. 5 μm thick bimetal cantilever current density

Rapid changes in current density occur while the cantilever beam is making large changes in displacement. Therefore, the two current density peaks in Figure 16 correspond to the rising and falling edges of the large displacement peak in Figure 13. The current is obtained by multiplying the current density by the cross-sectional area of the piezoelectric material. The cross-sectional area for all of the simulated designs is 200 μm^2.

Post-simulation data analysis yields the cantilever's generated power by multiplying the voltage data and the current data after scaling by the cross-sectional area. Figure 17 shows the instantaneous power generated by the 5 μm thick bimetal cantilever beam.

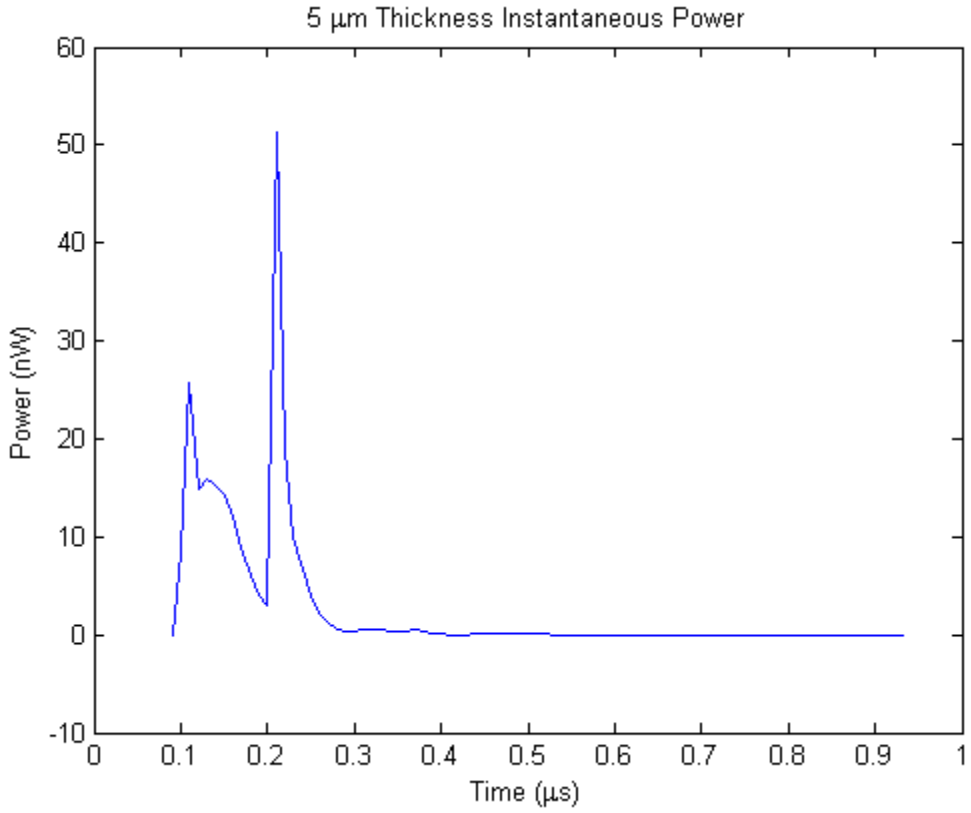

Figure 17. 5 μm thick bimetal cantilever instantaneous power

The range of time shown on the *x*-axis represents one cycle of operation. The first local maximum corresponds with the rising edge of the displacement peak in Figure 13; the absolute maximum corresponds with the falling edge of the displacement peak in Figure 13. Over one full cycle, the average power for the 5 μm thick bimetal cantilever is 1.95 nW. Most of the appreciable power generated by the cantilever beam occurs during the beginning of its cycle; this is the behavior of the cantilever beam at larger bimetal thicknesses. Therefore, it would be desirable to shorten the time length of a cycle to feature only the interval where appreciable power is generated by the cantilever beam. This issue is addressed through the down-scaling of the bimetal thickness. The next sub-section of this chapter shows the behavior of the cantilever beam at smaller bimetal thicknesses to exhibit the differences and benefits of scaling the thickness.

Smaller Bimetal Thicknesses

The results from the 1.5 μm bimetal thickness simulation are presented below to explain the behavior of the cantilever beam at smaller bimetal thicknesses. The smaller bimetal thicknesses performed much differently than the larger bimetal thicknesses. Although both follow the same principles of heating and then curling up, the mechanical response to the heat input function differs. This difference is evident in the cantilever tip displacement plot shown later in this sub-section. Because the mechanical response is different, it is expected that the electrical response is also different. This difference is evident in the voltage, current density, and instantaneous power plots shown later in this sub-section. Figure 18 shows the tip displacement of the cantilever beam for the 1.5 μm thick bimetal.

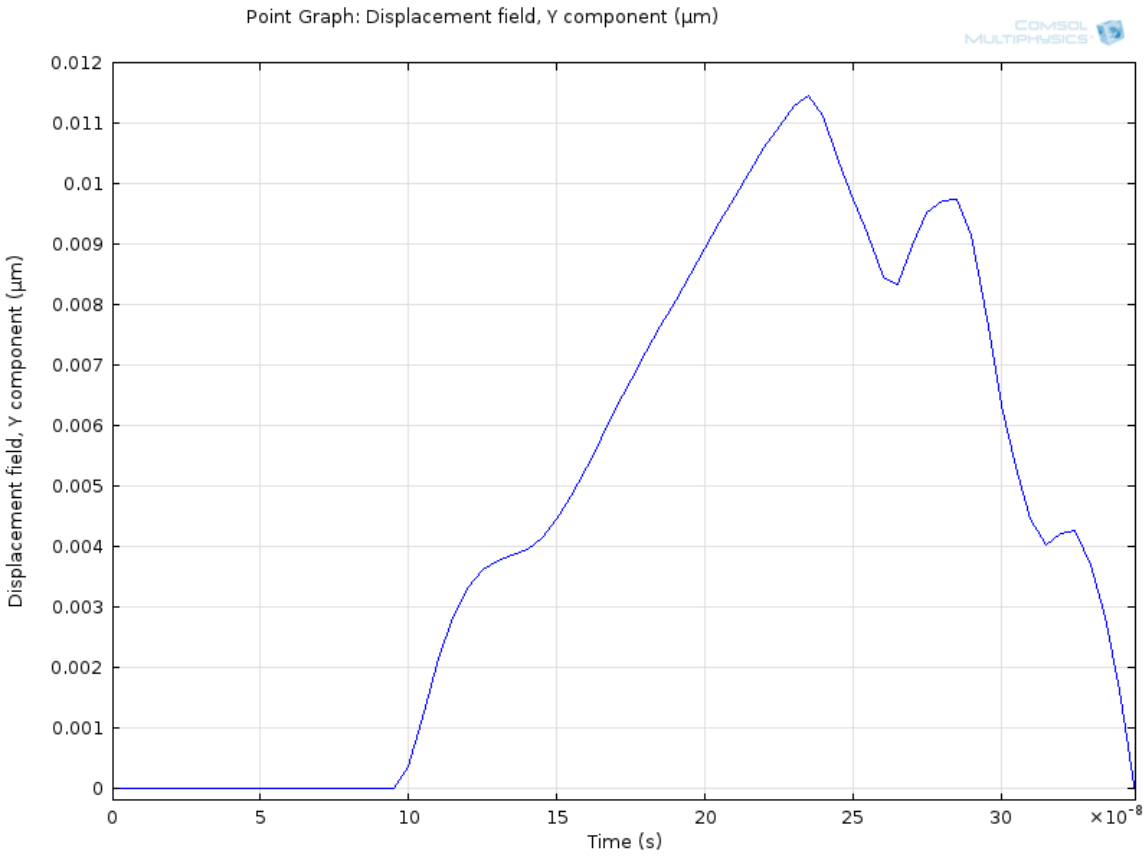

Figure 18. 1.5 µm thick bimetal cantilever tip displacement

Cantilever beams at smaller thicknesses display a displacement behavior consistent with the 1.5 µm thick bimetal simulation. In Figure 18, there is not one large initial displacement peak as seen in Figure 13. In Figure 18, the irregularity of the tip displacement indicates that multiple modal shapes influence the mechanical response of the cantilever beam to the heat input. For the cantilever beams at larger bimetal thicknesses, higher order modal shapes are negligible because the larger thickness resulted in a stiffer beam. For the cantilever beams at smaller bimetal thicknesses, higher order modal shapes are non-negligible because smaller bimetal thickness results in a less stiff beam. Additionally, the displacement cycle for the smaller bimetal thicknesses is

shorter than the displacement cycle of the larger bimetal thicknesses. A shorter displacement cycle ultimately results in a larger power output, which is discussed later in this sub-section.

The local maxima in the cantilever tip displacement plot, shown in Figure 18, correspond with the generated voltage from the piezoelectric material. Figure 19 shows the voltage recorded by Boundary Probe 1 in the 1.5 μm bimetal thickness simulation.

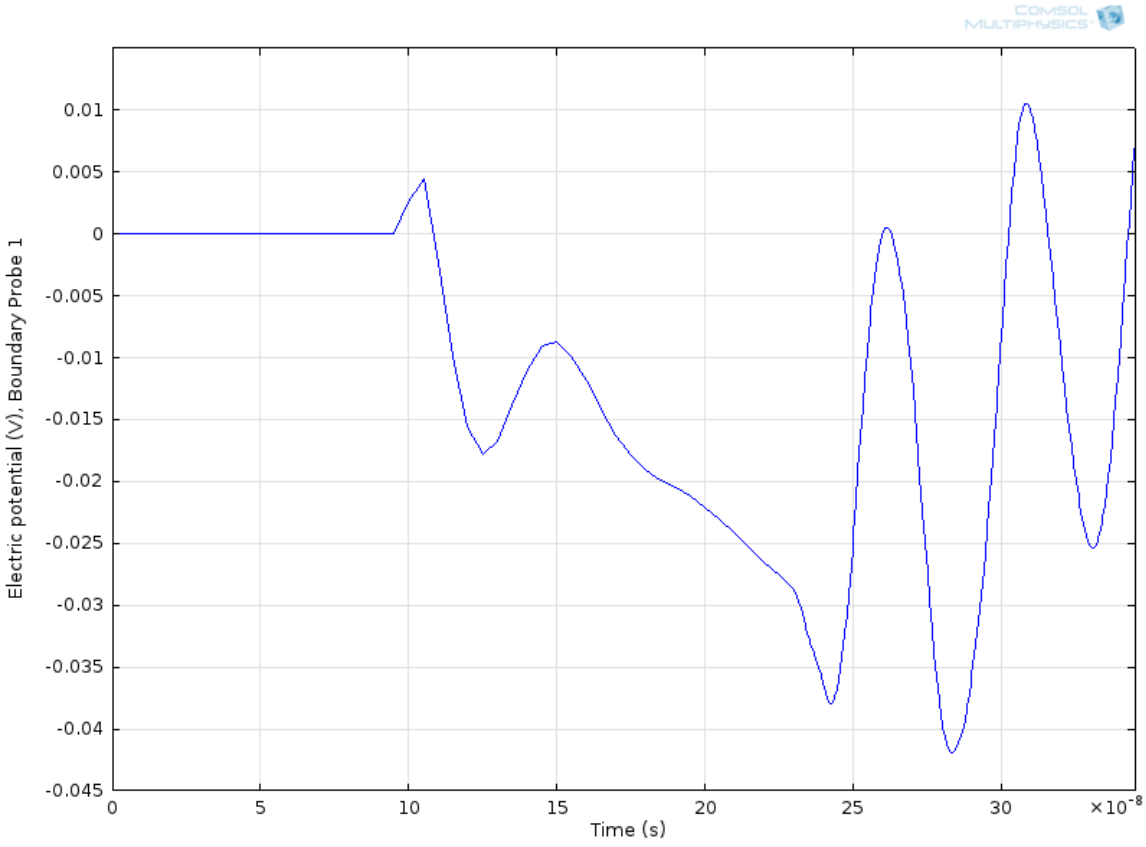

Figure 19. 1.5 μm thick bimetal cantilever voltage signal

The tuning process for the smaller bimetal thickness simulations is more difficult because there are multiple voltage magnitude peaks rather than one large definitive voltage magnitude peak. The tuning process is modified in the case of smaller bimetal

thicknesses to determine the length of the heating time that produces the largest voltage magnitude and reduces the amount of time where the voltage rises above zero. Figure 20 shows a surface plot of the electric potential through one vertical slice of the 1.5 μm bimetal thickness cantilever beam as it is stressed.

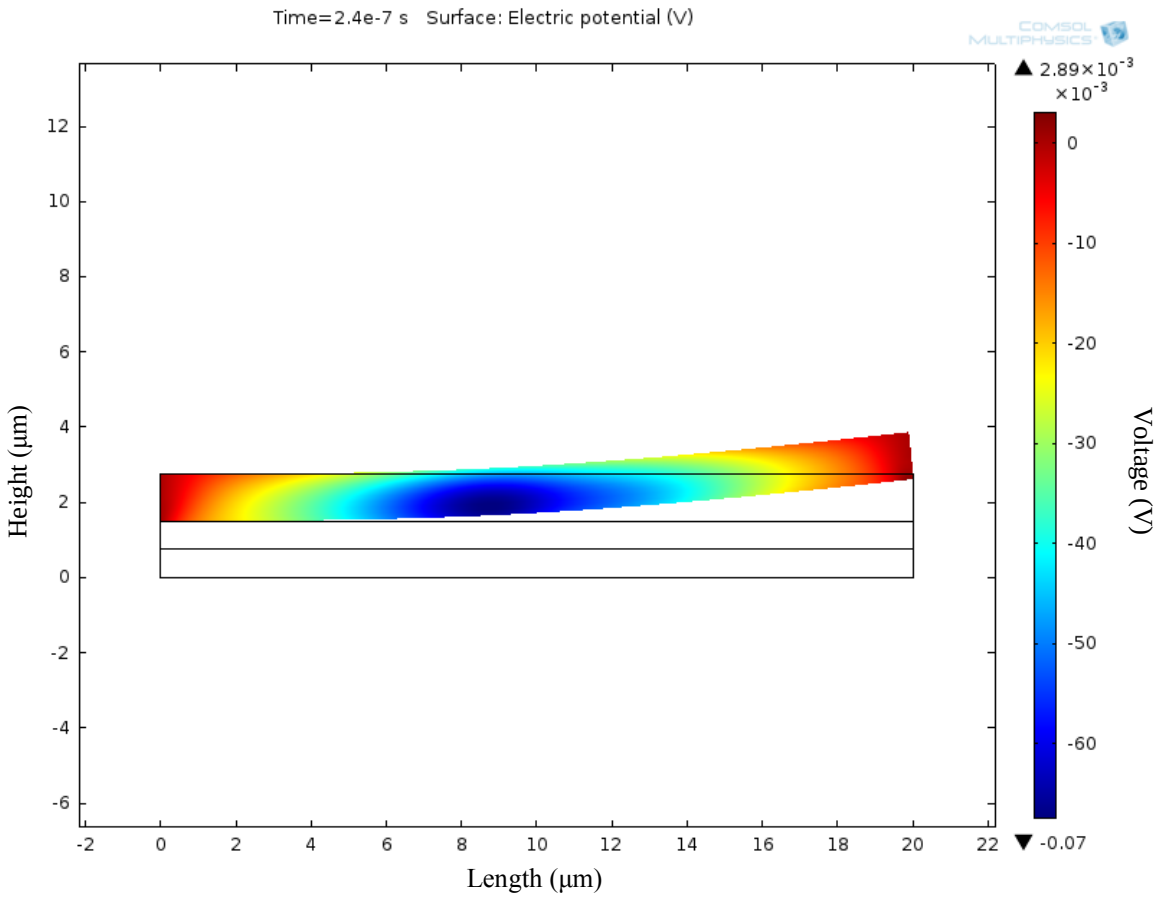

Figure 20. Stressed piezoelectric material (deformation scale 100; bimetal layer not shown)

Figure 20 is showing the state of the piezoelectric material at 0.24 μs, which is where the one of the local voltage magnitude maxima occurs. As can be noted from the color legend, the largest voltage magnitude is in the dark blue area at -0.07 V. In comparison to Figure 15, the location of the dark blue area has shifted in the negative

x-direction. In the same manner as the larger bimetal thickness simulations, the net voltage value is dropped across a 1 kΩ resistor using a virtual circuit.

The current density gives further evidence for the influence of higher order modal shapes due to its irregular nature. Figure 21 shows the current density of the piezoelectric material in the 1.5 μm bimetal thickness simulation.

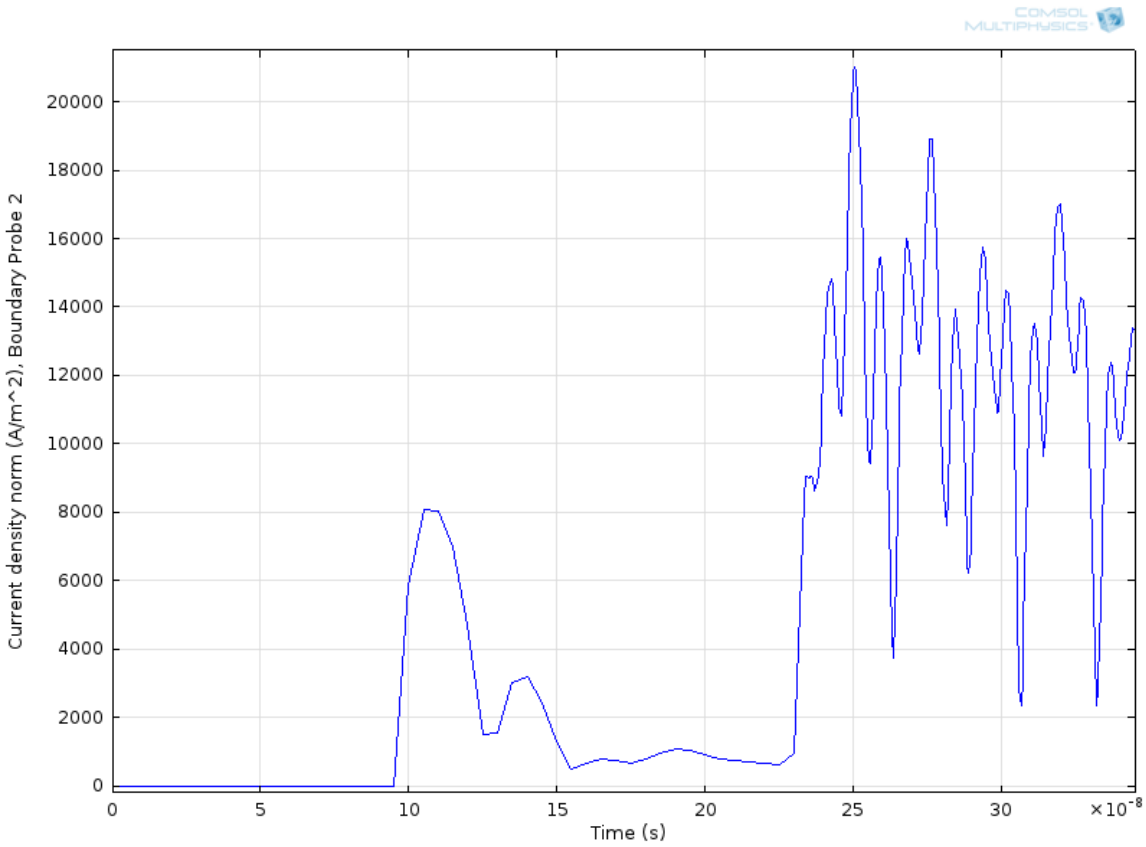

Figure 21. 1.5 μm thick bimetal cantilever current density

The rapid changes in current density occur while the cantilever beam is making large changes in displacement. Many peaks and troughs demonstrate the complex movement of the cantilever beam as the internal stresses within the piezoelectric material change quickly.

For smaller bimetal thicknesses, the cantilever's generated power is quite different from the generated power from the larger bimetal thicknesses. Figure 22 shows the instantaneous power generated by the 1.5 μm thick bimetal cantilever beam.

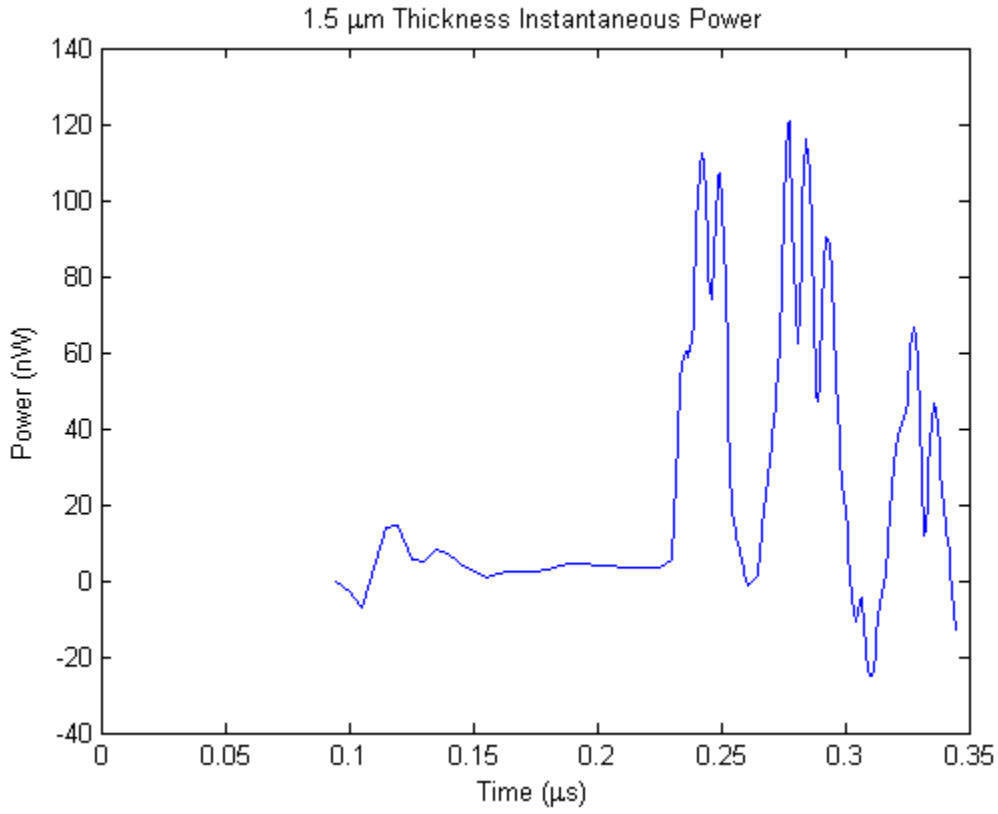

Figure 22. 1.5 μm thick bimetal cantilever instantaneous power

The range of time shown on the *x*-axis represents one cycle of operation; in this case, one cycle of operation is much shorter than seen in Figure 17. Over one full cycle, the average power for the 1.5 μm thick bimetal cantilever is 36.82 nW, which is over an order of magnitude greater than the average power from the 5 μm thick bimetal cantilever. Most of the appreciable power generated by the 1.5 μm thick bimetal cantilever beam occurs during the end of its cycle; this is the behavior of the cantilever

beam at smaller bimetal thicknesses. The length of one cycle has been shortened to an interval where a greater percentage on the cycle is spent generating appreciable power by the cantilever beam. This issue has been addressed through the down-scaling of the bimetal thickness.

Aggregate Results

Overall, the increase in output power from down-scaling the bimetal thickness is valid only until the point when the significance of higher order modal shapes interferes with appreciable power generation. For the design studied in this research, this occurs at around 1 μm thick for the bimetal. The three figures in this sub-section display the results for all simulations conducted in this research.

Figure 23 shows the peak voltage magnitude versus the bimetal thickness.

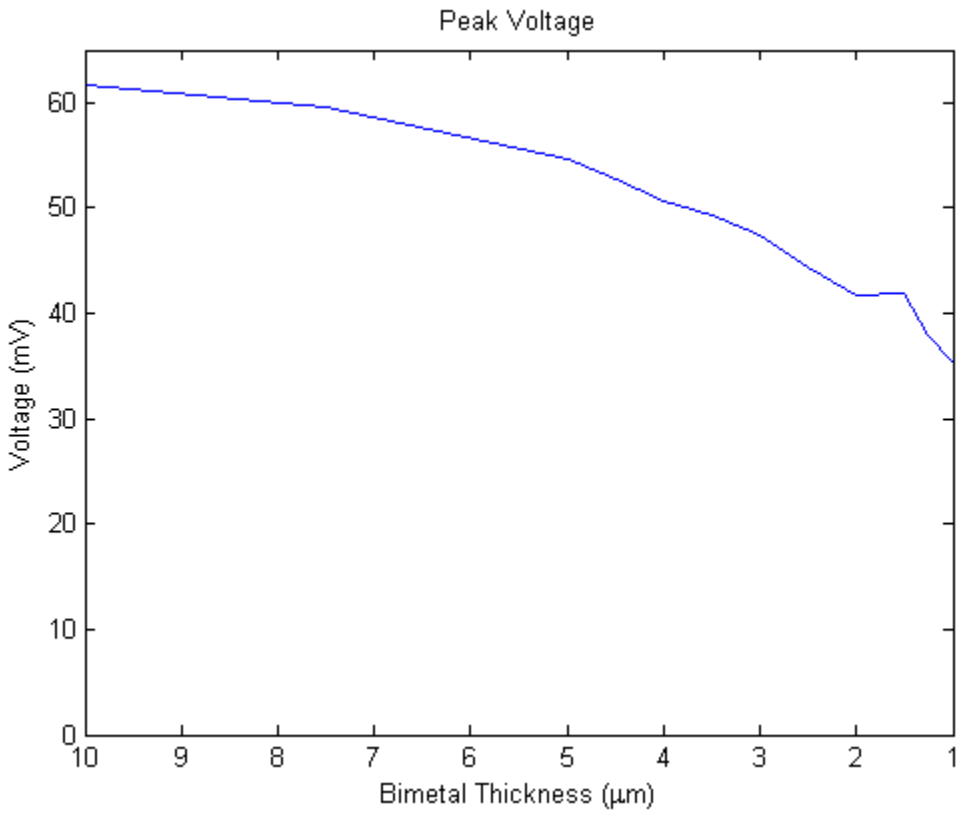

Figure 23. Peak voltage versus bimetal thickness across all simulations

The peak voltage decreases gradually as the bimetal thickness decreases. The piezoelectric material thickness is also decreased as the bimetal thickness is decreased to account for the change in deflection. Therefore, the relationship between the cantilever beam thickness and the peak voltage is expected to show a decrease in peak voltage as the thickness decreases. The peak voltage magnitude is not significantly influenced by the higher order modal shape effects.

While the peak voltage magnitude shows a steadily decreasing relationship, the cantilever beam frequency across all simulations indicates that there is a preferred range

to achieve higher frequencies. Figure 24 shows the cantilever beam frequency versus the bimetal thickness.

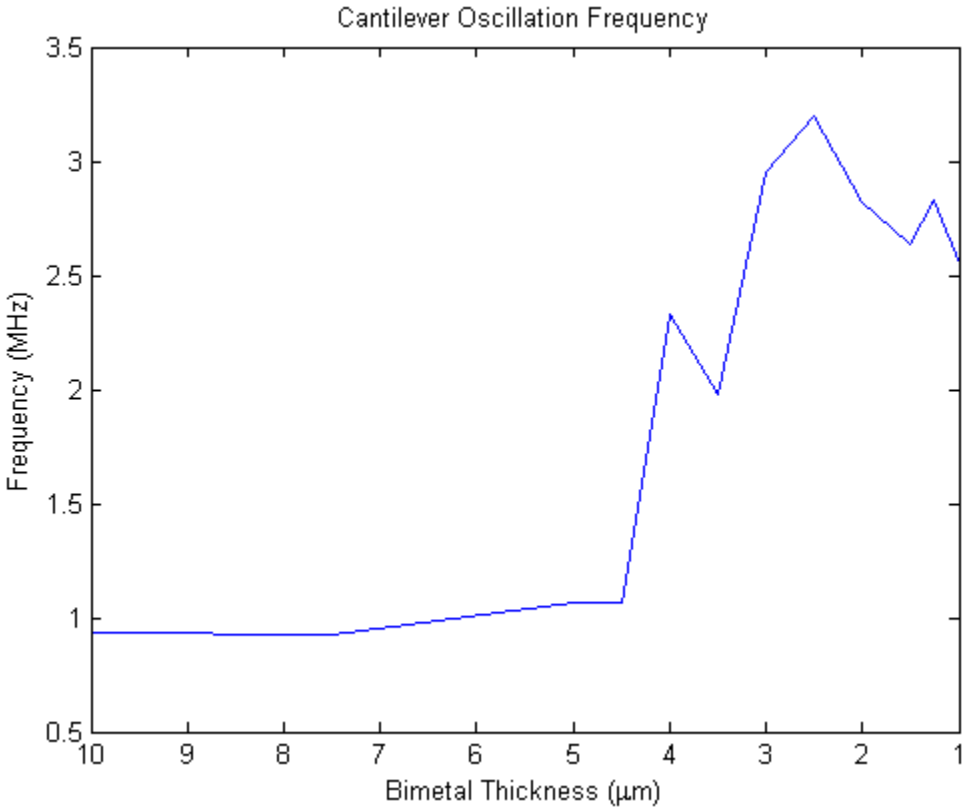

Figure 24. Cantilever beam frequency versus bimetal thickness across all simulations

The cantilever beam frequency reaches a maximum of 3.2 MHz at a bimetal thickness of 2.5 μm, and then begins to drop off upon further reduction of the bimetal thickness. The resonant frequency of each cantilever beam has an effect on how long the overall cantilever beam frequency is for one total displacement cycle. It is because of these resonant frequencies that the duty cycle changes as the bimetal thickness is decreased, but only to a certain point. The higher order modal shapes begin to interfere

with the operation of the cantilever beam and create diminishing returns for the cantilever beam frequency after reaching a bimetal thickness of 1.5 μm.

The average power generated displays a similar behavior to the cantilever beam frequency. Figure 25 shows the average electrical power versus the bimetal thickness.

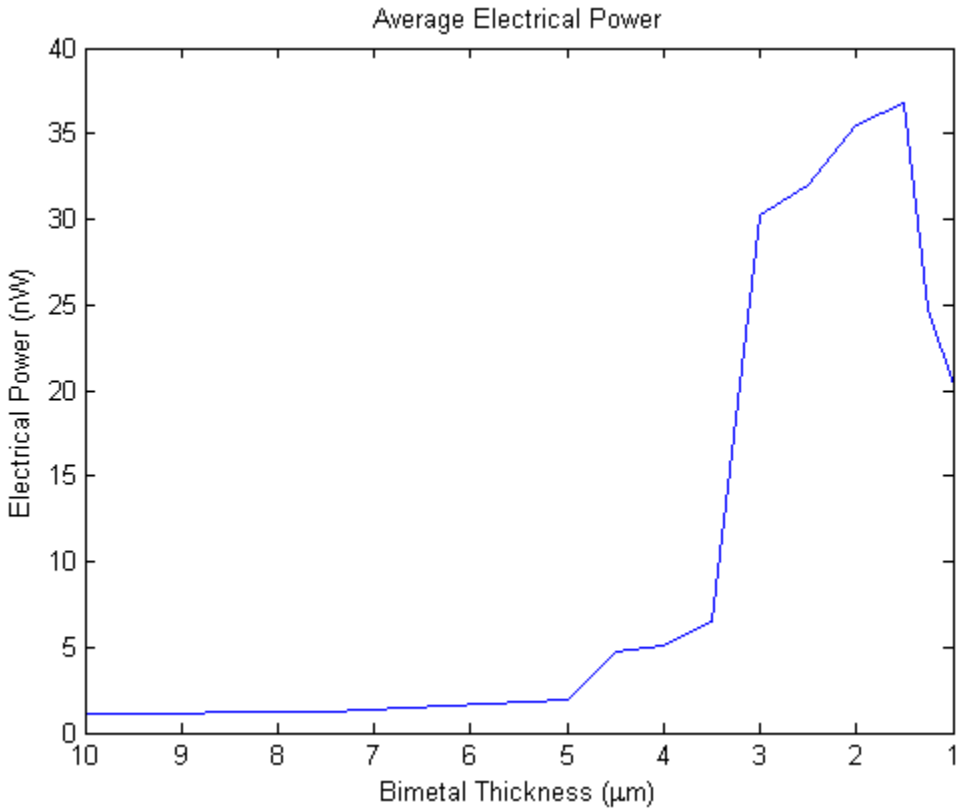

Figure 25. Average power versus bimetal thickness across all simulations

The average power recorded for each simulation in Figure 25 represents the average power generated for a single cantilever beam. Outside of simulation, it is expected that a real-world implementation of these devices would be in a large matrix of cantilever beams so that the power generated for each individual device would be summed using additional circuitry. The additional power management circuitry must be

designed to support non-synchronous devices in both series and parallel configurations. The initial response of the average power to the decreasing of the bimetal thickness is a significant increase in output power. But after reaching a bimetal thickness of 1.5 μm, the average power decreases sharply. Again, the higher order modal shapes prevent the continued increase of the average power as the bimetal thickness is decreased. At a bimetal thickness of 1.5 μm, the cantilever beam generates a maximum average power of 36.82 nW. From the perspective of a top-view, the cantilever dimensions in this design are 20 μm × 10 μm per device. A conservative estimate for device spacing in a matrix that allows for external circuitry would be 36 μm × 18 μm per device. By taking the maximum average power and dividing it by the conservative estimate for device spacing, the result is the average power density. This calculation yields an average power density of 5.68 mW/cm^2. This power density is two orders of magnitude higher than Seebeck devices recorded in the literature review, and it is comparable with the power densities that Puscasu reports in his research.

Summary

The campaign of experiments described in the test matrix from the chapter on methodology has been executed and yielded a sufficient data set from which to draw conclusions and recommend a superior dual-stage MEMS cantilever energy harvester that operates under the conditions of the human environment. The next chapter discusses the findings that emerge from this body of research and suggests avenues for future work.

V. Conclusions and Recommendations

Chapter Overview

This chapter states the findings that emerge from analyzing the results of this thesis research effort. Twelve different simulation experiments have been performed on a dual-stage MEMS cantilever energy harvester with the objectives of increasing the power density and improving the design. The following discussion relates the results of the campaign of experiments back to the original problem statement formed in the Introduction chapter of this document.

Design Configuration

The design configuration chosen in this research stems from the influence of non-Seebeck thermal harvesting devices found in the literature and the influence of piezoelectric vibration harvesting devices found in the literature [5]. The impact-based design is changed for the purpose of achieving a non-impact-based design with a higher power density than the impact-based design [28].

Thermal conduction occurs only when the bimetal is in contact with the hot side; the cold side of the device is entirely dependent on convection cooling from the ambient air. In the original design from the literature, the zero stress reference deposition temperature must be at the median of the total temperature differential; in the design used in this research, the zero stress reference deposition temperature must be at the temperature of the cold side.

Control Variables

The bimetal thickness scaling serves as the primary control variable in this research. The concept behind device scaling is drawn from the literature, which analytically shows that bimetal performance in a non-Seebeck energy harvesting system increases when the size of the device is decreased [2]. Although this research presents a modified design of the non-Seebeck design found in the literature, a similar phenomenon is found when scaling the bimetal thickness to a certain point. The conducted simulations demonstrate an increase in output power for the dual-stage MEMS cantilever energy harvester as the bimetal thickness is reduced until the thickness reaches about 1 μm. The characteristics of the device operation are discussed in this section.

At the two extremes of the spectrum of bimetal thicknesses tested, the electrical output decreases due to factors that negatively impact the device performance. At a bimetal thickness of 10 μm, the dual-stage MEMS cantilever energy harvester experiences decreased performance due to slow heating times. The bimetal layer thickness is such that the permeating heat from the contact area while the cantilever beam is latched takes extra time to affect the active layer of the bimetal. The latching time for the 10 μm bimetal thickness is 0.15 μs, which is the longest required latching time for the simulations conducted in this research. Slow heating time for the active layer decreases the frequency and therefore negatively impacts the device performance. One problem that occurs for smaller bimetal thicknesses is the influence of higher order modal shapes on the displacement response. Thinner cantilever beams are more susceptible to the effects of higher order modal shapes because the beam is more flexible. Higher order modal shapes reduce the voltage generated by the piezoelectric material due to the

creation of inflection points that separate convex and concave regions of the cantilever beam. Figure 26 shows an example of the piezoelectric material experiencing an inflection point in the 1 μm bimetal thickness simulation.

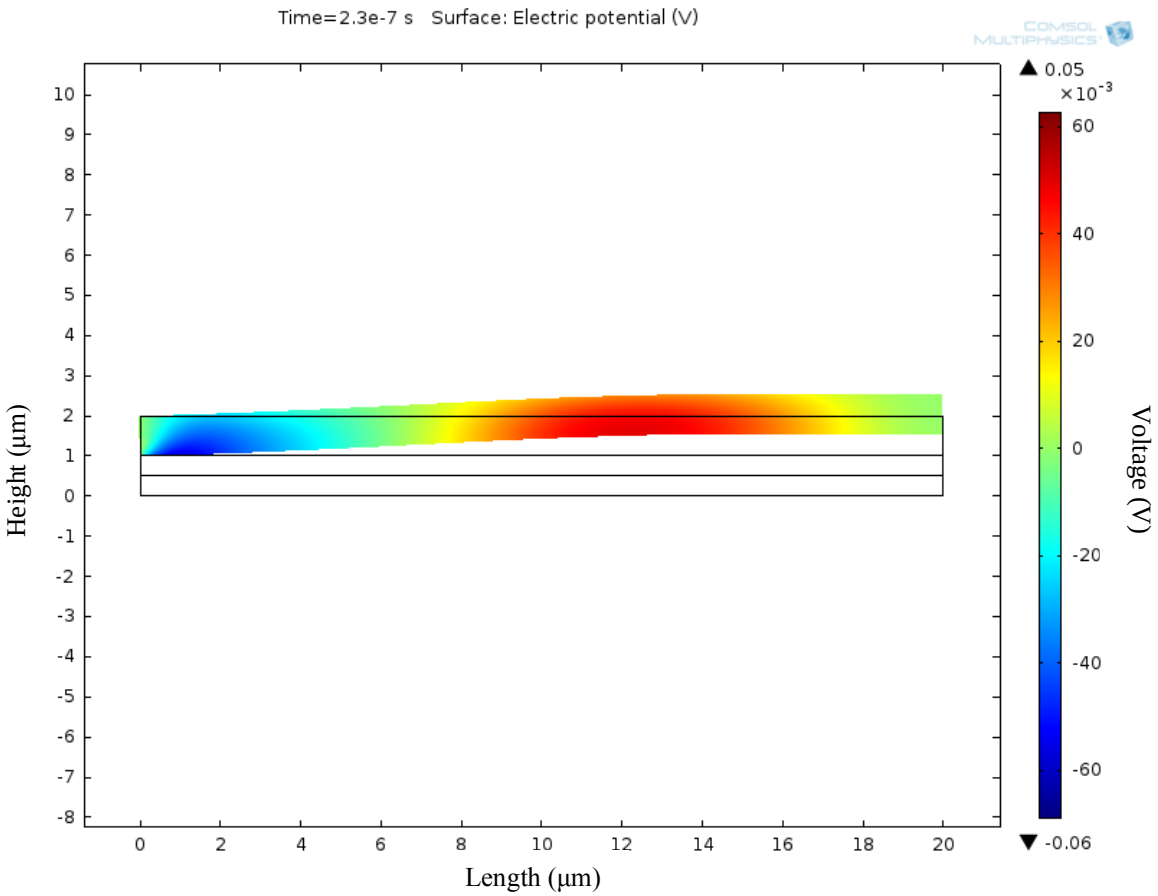

Figure 26. 1 μm bimetal thickness simulation experiencing an inflection point (bimetal not shown)

In Figure 26, the piezoelectric material experiences an inflection point at 0.23 μs into the simulation of the 1 μm bimetal thickness. Inflection points create localized regions of negative voltage and localized regions of positive voltage on the terminal of the piezoelectric material. These localized areas of negative and positive voltage cancel each other and reduce the net voltage output of the piezoelectric material. A reduction in

the voltage output of the piezoelectric material diminishes the overall electrical power output of the dual-stage MEMS cantilever energy harvester. Therefore, bimetals employed in the dual-stage MEMS cantilever energy harvester system suffer reductions in performance at thicknesses approaching 10 μm due to slow heating times and at thicknesses approaching 1 μm due to higher order modal shapes.

Latching time and PZT-5H thickness are controllable nuisance variables, in that they both depend on the bimetal thickness. In order to achieve the highest electrical output from the dual-stage MEMS cantilever energy harvester, the latching time must be individually tuned for each thickness to elicit the greatest electrical output. The primary goal of the latching time tuning process is to heat the cantilever beam long enough to create the largest peak voltage after the beam is released from contact. The secondary goal of the latching time tuning process is to create the shortest displacement cycle. For each thickness, the resonant frequency of the cantilever beam changes; this means that the overlaid underdamped response displays a different frequency and amplitude dependent on the thickness. The choice of latching time has a small effect on the displacement cycle of the dual-stage MEMS cantilever energy harvester. This interdependence complicates the process of choosing a latching time because in certain cases, a small sacrifice in voltage by lengthening or shortening the latching time results in a large change in the displacement cycle. Because the displacement cycle is directly linked to the operating frequency, the small change in latching time can ultimately result in an improved electrical power output. This behavior is dependent on the overlaid underdamped displacement response, which changes with each bimetal thickness and becomes very irregular due to higher order modal shape influences as the bimetal

thickness approaches 1 μm. The recommendation for finding the optimal latching time is to fabricate and test different latching voltages and characterize the electrical output power of the real system versus latching voltage.

Significance of Research

The end-goal of this line of research is to enable a wearable thermal energy harvesting device that functions as a mobile power supply able to power small electronics. A device with this capability would benefit the warfighter who is deployed into a remote area without access to the power grid. Instead of being forced to carry heavy batteries, the warfighter could carry a thermal energy harvesting device to power his or her electronics. This thesis research effort contributes toward this goal by adapting designs found in the literature and exploring alternate configurations in the simulation environment to recommend a design that functions under the constraints of human body heat and ambient air. This research applies the analytical findings from the literature and tests them in the simulation environment. All experiments in this research effort were conducted in simulation with the underlying objective being that a superior design that fits the presented conditions would be recommended.

Recommendations for Future Research

The concerns for future research from the perspective of this thesis are split into two categories. There exists future simulation research for the alternate configurations presented in this research. There are many different future research options involving the fabrication and testing of prototype dual-stage MEMS cantilever energy harvester devices that fit the constraints of the human body's environment.

For future simulation research, the temperature differential has a unique effect on the operation of the dual-stage MEMS cantilever energy harvester. In this research effort, the temperature differential was held constant at 10 °C between 33 °C and 23 °C. Future research could address the external conditions of extreme hot/cold weather and suggest an optimal temperature range of operation for the device. Additionally, the use of different materials and the alteration of other geometric parameters would prove valuable for further design optimization.

For future fabrication and testing research, the recommendations presented in this body of research need to be fabricated and tested for feasibility. A reliable fabrication process for creating a large matrix of dual-stage MEMS cantilever energy harvesters in a small area needs to be developed. Power management circuitry that supports large matrices of non-synchronous device operation while accounting for possible parasitic capacitances is an important direction for future research. Likewise, human subject testing for device performance must also take place to determine the power characteristics of the dual-stage MEMS cantilever energy harvester under the real-world conditions of the human body. Using the conclusions gathered from simulation, the conclusions gathered from fabrication, the conclusions gathered from power management circuitry development, and the conclusions gathered from human subject testing, a final design can be reached and ultimately implemented.

Additional challenges exist for using the power generated by the dual-stage MEMS cantilever energy harvester because voltage peaks less than 100 mV in magnitude are too low for traditional voltage rectification methods [1]. Fortunately, most of the time the voltage signals recorded in the simulations for this research stayed negative and did

not go above zero. Boost converters or bootstrapping methods may be options for achieving higher voltages. One of the power conditioning circuits suggested by Chao might be a good choice to efficiently convert the energy from the dual-stage MEMS cantilever energy harvester [30]. Additionally, a mechanical diode-less voltage multiplier is a viable option [31]. Power conditioning is an important part of the future research required in this area because the full realization of the total power available in a large matrix of dual-stage MEMS cantilever energy harvesters cannot be reaped if an efficient method for aggregating the individual power from each device is not implemented.

Summary

Small-scale thermal energy harvesting has been a steadily growing field of research for decades, and there are a nearly endless number of ways that these systems can be integrated into modern life. Using a dual-stage MEMS cantilever energy harvester for the harvesting of human body heat is a unique niche that requires continued research for the purpose of creating a complete functional system in the future.

Appendix

Included in this appendix are additional equations from the analytical derivation referenced in the Literature Review that were not used in the Derivation sub-section but provided further insight into the operation of the devices studied by Puscasu *et al.* The authors compiled and derived a list of equations that serve as an analytical foundation for the operation of bimetal and piezoelectric based energy harvesters [2]. A sample of the relevant equations is given to provide the mathematical context for dual-stage non-Seebeck thermal energy harvesters. Bimetal heating and cooling constitutes the primary stage of thermal to mechanical energy conversion. The bimetal internal average temperature, dependent on time, is expressed as:

$$\overline{T}(t) = \frac{8}{\pi^2}\exp\left(-\pi^2 \alpha_T \frac{t}{L^2}\right)\left(T_{cold} - T_{hot}\right) + T_{hot} \tag{32}$$

where α_T is the average thermal diffusivity of the bimetal materials, L is the length of the bimetal, T_{cold} is the temperature of the cold side, and T_{hot} is the temperature of the hot side. Based on the temperature of the bimetal, induced thermal stress within the bimetal generates accumulated elastic energy. The bimetal elastic energy is expressed as:

$$E_{elast} = \frac{Y}{32}\left(\alpha_2 - \alpha_1\right)^2 \Delta T^2 V_b \tag{33}$$

where Y is the average Young's Modulus of the materials, α_2 is the larger coefficient of thermal expansion (CTE), α_1 is the smaller CTE, ΔT is the temperature differential, and V_b is the volume of the bimetal. The elastic energy accumulation is

released when the bimetal snaps between its two stable states. The bimetal kinetic energy represents the release of its elastic energy and is expressed as:

$$E_k = \frac{\rho V_b \times v^2}{2} \tag{34}$$

where ρ is the density of the materials, V_b is the volume of the bimetal, and v is the maximum speed of the bimetal during the snap action. The kinetic energy of the bimetal causes a deflection of the piezoelectric material when the two components make contact.

Bibliography

[1] N. S. Hudak, "Small-scale energy harvesting through thermoelectric, vibration, and radiofrequency power conversion," *J. Appl. Physics*, vol. 103, no. 10, p. 101301, 2008.

[2] O. Puscasu, "Scale laws for enhanced power for MEMS based heat energy harvesting," *IEEE Silicon Nanoelectronics Workshhop (SNW)*, pp. 1-2, 2012.

[3] O. Puscasu, "An innovative heat harvesting technology (HEATec) for above-Seebeck performance," *IEEE Electron Devices Meeting (IEDM)*, pp. 12.5.1-12.5.4, 2012.

[4] O. Puscasu, "A disruptive technology for thermal to electrical energy conversion," *Microelectronics J.*, vol. 45, pp. 554-558, 2014.

[5] O. Puscasu, "Flexible bimetal and piezoelectric based thermal to electrical energy converters," *Sensors and Actuators A: Physical*, vol. 214, pp. 7-14, 2014.

[6] E. Sardini, "Passive and Self-Powered Autonomous Sensors for Remote Measurements," *IEEE Sensors J.*, vol. 9, pp. 943-960, 2009.

[7] V. G. Krishnan, "Design and scaling of microscale Tesla turbines," *J. Micromech. and Microeng.*, vol. 23, p. 125001, 2013.

[8] S. J. Elliott, "Scaling of electromagnetic transducers for shunt damping and energy harvesting," *J. Sound and Vibration (JSV)*, vol. 333, pp. 2185-2195, 2014.

[9] X. Xie, "A ring piezoelectric energy harvester excited by magnetic forces," *Int. J. Eng. Sci.*, vol. 77, pp. 71-78, 2014.

[10] J. Lin, "Surface Micromachined MEMS Capacitors With Dual Cavity for Energy Harvesting," *J. Microelectromech. Syst.*, vol. 22, pp. 1458-1469, 2013.

[11] M. Bao, "Squeeze film air damping in MEMS," *Sensors and Actuators A: Physical*, vol. 136, pp. 3-27, 2007.

[12] Y. Arakawa, "Micro Seismic Power Generator Using Electret Polymer Film," *Fourth International Workshop on Micro and Nanotechnology for Power Generation and Energy Conversion Applications,* pp. 187-190, 2004.

[13] N. S. Shenck, "Energy Scavenging with Shoe-Mounted Piezoelectrics," *IEEE Micro,* vol. 21, no. 3, pp. 30-42, 2001.

[14] R. Caliò, "Piezoelectric Energy Harvesting Solutions," *Sensors J.,* vol. 14, no. 3, pp. 4755-4790, 2014.

[15] E. Varadrajan, "Design and Simulation of Unimorph Piezoelectric Energy Harvesting System," *2013 COMSOL Conference Proceedings,* pp. 1-6, 2013.

[16] S. Boisseau, "Cantilever-based electret energy harvesters," *Smart Materials and Structures,* vol. 20, no. 10, pp. 1-11, 2011.

[17] H. Böttner, "Thermoelectric Micro Devices: Current State, Recent Developments and Future Aspects for Technological Progress and Applications," *Twenty-First International Conference on Thermoelectrics,* pp. 511-518, 2002.

[18] H. Böttner, "New Thermoelectric Components Using Microsystem Technologies," *J. Microelectromech. Syst.,* vol. 13, no. 3, pp. 414-420, 2004.

[19] H. Glosch, "A thermoelectric converter for energy supply," *Sensors and Actuators A: Physical,* vol. 74, no. 1-3, pp. 246-250, 1999.

[20] R. Venkatasubramanian, "Thin-film thermoelectric devices with high room-temperature figures of merit," *Nature,* vol. 413, no. 6856, pp. 597-602, 2001.

[21] S. Dalola, "Autonomous Sensor System with RF Link and Thermoelectric Generator for Power Harvesting," *IEEE International Instrumentation and Measurement Technology Conference,* pp. 1376-1380, 2008.

[22] S. Boisseau, "Semi-flexible bimetal-based thermal energy harvesters," *Smart Materials and Structures,* vol. 22, no. 2, pp. 1-8, 2013.

[23] V. Leonov, "Thermoelectric Energy Harvesting of Human Body Heat for Wearable Sensors," *IEEE Sensors J.,* vol. 13, pp. 2284-2291, 2013.

[24] S. Monfray, "Innovative thermal energy harvesting for zero power electronics," *IEEE Silicon Nanoelectronics Workshop (SNW)*, pp. 1-4, 2012.

[25] S. Boisseau, "Bimetal-and-electret-based thermal energy harvesters - Application to a battery-free Wireless Sensor Node," *Instrumentation and Detectors*, pp. 1-12, 2013.

[26] A. Arrnaud, "Piezoelectric and electrostatic bimetal-based thermal energy harvesters," *J. Phys. Conf. Ser.*, vol. 476, no. 1, pp. 1-5, 2013.

[27] K. B. Lee, Principles of Microelectromechanical Systems, Hoboken, NJ: John Wiley & Sons, Inc., 2011.

[28] C.-N. Xu, "Electrical Power Generation Characteristics of PZT Piezoelectric Ceramics," *IEEE Transactions on Ultrasonics, Ferroelectrics, and Frequency Control*, vol. 45, no. 4, pp. 1065-1070, 1998.

[29] D. Berlincourt, "Properties of Morgan Electro Ceramic Ceramics," *Technical Publication TP-226*, pp. 1-12, 2002.

[30] P. C.-P. Chao, "Energy Harvesting Electronics for Vibratory Devices in Self-Powered Sensors," *IEEE Sensors J.*, vol. 11, pp. 3106-3121, 2011.

[31] F. Giusa, "A diode-less mechanical voltage multiplier: A novel transducer for vibration energy harvesting," *Sensors and Actuators A: Physical*, vol. 212, pp. 34-41, 2014.

Vita

Education

B.S., Electrical & Computer Engineering, 2013, Norwich University, Northfield, VT

M.S., Electrical Engineering, Expected, Air Force Institute of Technology, WPAFB, OH

Association Memberships

IEEE, Tau Beta Pi, Eta Kappa Nu

Publications & Papers

"Energy Harvesting & Recapture from Human Subjects: Dual-Stage Thermal MEMS Energy Converter," *RSAMD 2014 Conference Proceedings*, (Pending)

"Microelectronics Thermal Management using Microelectromechanical Systems (MEMS) Bimorph Cantilever Beams (MBCB)," *Sensors & Actuators: A Physical*, (Pending)

REPORT DOCUMENTATION PAGE

Form Approved
OMB No. 074-0188

1. REPORT DATE *(DD-MM-YYYY)*	2. REPORT TYPE	3. DATES COVERED *(From – To)*
26-03-2015	Master's Thesis	August 2013 – March 2015

TITLE AND SUBTITLE
Energy Harvesting & Recapture from Human Subjects:

Dual-Stage MEMS Cantilever Energy Harvester

5a. CONTRACT NUMBER

5b. GRANT NUMBER

5c. PROGRAM ELEMENT NUMBER

6. AUTHOR(S)

Sullivan, Nicholas P., Second Lieutenant, USAF

5d. PROJECT NUMBER

5e. TASK NUMBER

5f. WORK UNIT NUMBER

7. PERFORMING ORGANIZATION NAMES(S) AND ADDRESS(S)
Air Force Institute of Technology
Graduate School of Engineering and Management (AFIT/EN)
2950 Hobson Way, Building 640
WPAFB OH 45433-8865

8. PERFORMING ORGANIZATION REPORT NUMBER

AFIT-ENG-MS-15-M-068

9. SPONSORING/MONITORING AGENCY NAME(S) AND ADDRESS(ES)

Intentionally left blank

10. SPONSOR/MONITOR'S ACRONYM(S)

Unsponsored N/A

11. SPONSOR/MONITOR'S REPORT NUMBER(S)

Unsponsored N/A

12. DISTRIBUTION/AVAILABILITY STATEMENT
DISTRUBTION STATEMENT A. APPROVED FOR PUBLIC RELEASE; DISTRIBUTION UNLIMITED.

13. SUPPLEMENTARY NOTES
This material is declared a work of the U.S. Government and is not subject to copyright protection in the United States.

14. ABSTRACT

Recent thermal energy harvesting research has advanced alternative non-Seebeck devices and shifted attention towards applications with low temperature differentials near ambient. This research effort takes a simulation-based approach to improve the performance of a modified dual-stage MEMS cantilever energy harvester. The device employs a bimetal and a piezoelectric transducer to harvest energy from a 10 °C temperature differential. The proposed application for the device is as a wearable energy harvester, capable of generating power from the human body using skin temperature (average 33 °C) as the hot side and ambient air (23 °C) as the cold side. A bimetal thickness scaling study is conducted, in which the 1.5 μm thickness yields the maximum electrical power output of 36.82 nW per device. This translates to a power density of 5.68 mW/cm^2, which surpasses the performance of many Seebeck and non-Seebeck designs from the literature.

15. SUBJECT TERMS
Energy Harvesting, MEMS, Bimetal, Piezoelectric, Thermal, Heat Engine, Bioengineering

16. SECURITY CLASSIFICATION OF:			17. LIMITATION OF ABSTRACT	18. NUMBER OF PAGES	19a. NAME OF RESPONSIBLE PERSON
a. REPORT	b. ABSTRACT	c. THIS PAGE			Dr. Brett Borghetti, AFIT/ENG
U	U	U	UU	100	19b. TELEPHONE NUMBER *(Include area code)* (937) 785-6565, ext 4612 (Brett.Borghetti@afit.edu)

Standard Form 298 (Rev. 8-98)
Prescribed by ANSI Std. Z39-18